Design Rules for Biomolecular Adhesion: Lessons from Force Measurements

Deborah Leckband

Department of Chemical and Biomolecular Engineering, University of Illinois, Urbana-Champaign, Illinois 61801; email: leckband@illinois.edu

Annu. Rev. Chem. Biomol. Eng. 2010. 1:365–89

First published online as a Review in Advance on March 9, 2010

The *Annual Review of Chemical and Biomolecular Engineering* is online at chembioeng.annualreviews.org

This article's doi: 10.1146/annurev-chembioeng-073009-100931

1947-5438/10/0715-0365$20.00

Key Words

surface force apparatus, atomic force microscopy, nanomechanics, steered molecular dynamics, catch bonds

Abstract

Cell adhesion to matrix, other cells, or pathogens plays a pivotal role in many processes in biomolecular engineering. Early macroscopic methods of quantifying adhesion led to the development of quantitative models of cell adhesion and migration. The more recent use of sensitive probes to quantify the forces that alter or manipulate adhesion proteins has revealed much greater functional diversity than was apparent from population average measurements of cell adhesion. This review highlights theoretical and experimental methods that identified force-dependent molecular properties that are central to the biological activity of adhesion proteins. Experimental and theoretical methods emphasized in this review include the surface force apparatus, atomic force microscopy, and vesicle-based probes. Specific examples given illustrate how these tools have revealed unique properties of adhesion proteins and their structural origins.

1. INTRODUCTION

SMD: steered molecular dynamics

Cell adhesion is essential for the organization and homeostasis of all multicellular organisms. Apart from maintaining mechanical connections between cells and matrix or other cells, adhesion proteins carry out a host of functions that specifically modulate mechanical connections within different biological contexts. Exploiting or altering these functions is the focus of engineering applications including tissue engineering, drug design, and wound healing. The molecular design rules underlying the unique structure/function relationships of these specialized molecules may also inform the biomimetic design of, for example, targeted drug carriers.

Broadly, adhesion proteins perform specific functions that are linked to their different dynamic, mechanical environments. Some protein families, such as the classical cadherins—calcium-dependent intercellular adhesion proteins—maintain stable cell–cell junctions that often perform critical barrier functions. Examples include desmosomal junctions in skin and tight intercellular junctions in the vascular endothelium or in the intestinal epithelium. Cadherin structures facilitate the assembly, stability, and regulated remodeling of these specialized cell–cell junctions. Conversely, selectins, which are members of the C-type lectin family that are expressed on vascular endothelial cells, efficiently capture rapidly circulating cells in the bloodstream. Selectin function requires both rapid tether formation and the capacity to modulate cell adhesion and rolling on the endothelium under different fluid flow conditions. Other C-type lectins recognize pathogen-specific ligand patterns, enabling professional killer cells to bind to and neutralize infectious agents. Another major adhesion protein family, integrins, form both static and dynamic cell matrix adhesions in both adherent (static) and motile cells. They also function as tension sensors to modulate cell contractility in response to changes in the mechanical environment.

This functional diversity is linked to the variety of adhesion protein structures, and an overarching challenge is to define the relationships between the protein structures and their response to dynamically varying forces. The forces required to manipulate or control proteins are too small to detect by conventional methods. The development of sensitive experimental techniques was essential to interrogating the mechanical properties of proteins and determining the unique workings of these molecular machines. The nanomechanical measurements now available have revealed novel molecular properties linked to protein architectures that would not be detected from solution binding studies or crystal structures.

This review highlights experimental and theoretical approaches that have enabled the identification of molecular design rules underlying the specialized functions of adhesion proteins. In particular, I focus on examples in which the dynamic response to force or the complexity of the binding interactions could not be predicted from crystal structures or identified by solution binding measurements. Central issues are the interplay between protein architecture, the protein confinement to cell surfaces, and the mechanism and dynamics of adhesion.

2. ATOMISTIC SIMULATIONS OF FORCE-INDUCED BOND RUPTURE

What is the relationship between adhesion and bond chemistry? This is one of the most basic questions of biomolecular adhesion. Steered molecular dynamics (SMD) simulations provide a powerful approach to obtaining atomic-level insight into the structural basis of the mechanical functions of proteins (1–9). Simulations of cell adhesion molecules can identify key physical interactions that stabilize receptor-ligand bonds under force. Examples include immune proteins CD2 and CD58 (5), the neural cell adhesion molecule (1), cadherin (6), selectins (3, 4), and integrins (2, 9). Related studies identified changes that modulate cell adhesion, including the force-induced exposure of cryptic binding sites in extracellular matrix proteins and actin-binding proteins

(10, 11). Increasingly, comparisons with experiments demonstrate the predictive value of these simulations and identify atomic-level interactions underlying force-dependent structural changes or bond strengths (12). The range of biophysical applications of SMD is reviewed elsewhere (12). The following discussion focuses on examples that reveal unique aspects of adhesive protein functions.

SMD simulations monitor the evolution of macromolecular structures subject to an applied force and follow force-induced conformational changes on timescales up to tens of nanoseconds, as in other molecular dynamics approaches. In the simulations, the molecules or complexes are pinned at one end and force is applied to a second terminus, during which conformational changes are followed in (simulation) time. The force-time history can be applied in different ways, but two main approaches have been used to study adhesion molecules. First, simulations at constant pulling velocity fix one end of the complex, and the end of the second molecule is attached to a harmonic spring, which is translated at constant velocity. The computed force-time trajectory exhibits small jumps signifying intramolecular and intermolecular bond ruptures. The final drop to zero force occurs upon final separation. Analyses of bond formation and rupture, as a function of the simulation time and total applied force, identify bonds sustaining the highest loads and hence those most critical for adhesion.

Second, the constant force method applies to the complex a constant force that is below the rupture threshold and allows thermal fluctuations to drive complex dissociation (5). In this case, the end-to-end complex length remains constant until small bonds break and the protein adjusts to a new configuration. The lifetime of each configuration defines the persistence of each force-time plateau. Subsequent step changes between plateaus occur until the complex finally separates. Comparisons of the simulations under the different pulling conditions test whether the force-dependent unbinding trajectory is independent of the force history.

CD2 and CD58 are proteins in adaptive immunity that facilitate interactions between thymus cells (T cells) and antigen-presenting cells (APCs) (13, 14). CD2 is found on T cells, and its ligands are expressed on APCs. Structures of CD2 and of its ligands, rat CD48 (15–18), and human CD58 (18, 19), as well as biochemical data (20), suggest that CD2 binds its ligands in a head-to-head configuration that is stabilized by multiple salt bridges at the binding interface (**Figure 1*A***) (14).

SMD simulations of the forced unbinding of the complex between the outer domains of CD2 and CD58 investigated the role of the salt bridges in CD2 adhesion (5). At constant pulling velocity, sharp drops in force-time trajectories signify the rupture of noncovalent bonds under different forces (**Figure 1*B***). Snapshots of the complex revealed that these discontinuities (**Figure 1*C***) are due to the failure of salt bridges at the protein–protein interface under different applied forces. Bonds rupturing late at higher forces withstand greater forces, whereas those breaking early are not load-bearing contacts. These simulations both confirmed that salt bridges are load-bearing contacts and identified the bonds that are most critical for the mechanical stability of the CD2-CD58 complex. The simulations also identified a transient salt bridge that impeded complex disruption but was not seen in the crystal structure. The predicted roles of the different charged amino acids in CD2 were subsequently confirmed experimentally in surface force apparatus (SFA) measurements with CD2 charge mutants (21).

SMD studies of integrin activation also identified a possible molecular mechanism of integrin activation by opening a key hinge region (22). Earlier work suggested that a water bridge stabilizes integrin-RGD [arginine (R)-glycine (G)-aspartate (D)] bonds under force (2). Simulations of the forced detachment of neural cell adhesion molecules (NCAMs) clarified the roles of salt bridges in homophilic NCAM adhesion and reconciled apparent disparities between different NCAM crystal structures (1). Studies of selectin-carbohydrate interactions suggest that ligand sliding over

Conformational changes: structural changes in a folded macromolecule that accompany a change from one stable configuration to a second configuration

SFA: surface force apparatus

NCAM: neural cell adhesion molecule

a surface of the selectin and force-dependent conformational changes may underlie the catch bond behavior of selectins (3), (4).

Catch bonds: noncovalent bonds in which the dissociation rate, which is inversely proportional to the lifetime, decreases with increasing force on the bond

SHD: Szabo Hummer Dudko

The short simulation timescale (tens of nanoseconds) relative to experimental timescales is often perceived as a limitation of SMD. However, the increasing number of experimental studies that have confirmed simulation predictions attests to the value of SMD in predicting key interactions and mechanisms underlying passive protein responses to force (12). Semi-quantitative, atomistic details of unbinding processes have accurately predicted key interactions and functionally relevant conformational changes in several cases, demonstrating the value of SMD in understanding the structural basis of the passive mechanical properties of proteins.

3. TENSILE STRENGTHS OF SINGLE PROTEIN BONDS

Single bond rupture measurements are now commonly used to investigate the properties of noncovalent bonds. They are also the most appropriate experimental system for testing SMD predictions of receptor-ligand bond rupture. Such studies of receptor-ligand bonds are too numerous to cite here. This review instead focuses on results that are directly relevant to cell adhesion and the functional insights they provide.

3.1. Physical Models of Bond Rupture: Relating Force to Bond Chemistry

A goal of single bond rupture is to extract kinetic and mechanistic details underlying the passive responses of protein bonds to force. The information content lies in the relationship between force, dissociation rate, bond chemistry, and the protein structure. Three main experimental approaches are used to rupture single protein bonds: (*a*) rupture under a steadily increasing force or force ramp, $dF/dt = r_F$; (*b*) bond rupture under constant force; or (*c*) bond rupture following an abrupt force jump and subsequent, steady force ramp (**Figure 2**).

Different models relating bond rupture forces to bond chemistry have been proposed by Bell (23), by Evans and Ritchie (24), and by Szabo, Hummer, and Dudko (SHD) (25). The unifying concept is that force applied to a bond accelerates the dissociation rate by lowering the activation free energy for unbinding G^{ts}. Model differences lie in assumptions about the intermolecular potential, how force modifies the position of the transition state, the analytical expression for the dissociation rate, and its relationship to force. Bell predicted that force alters dissociation rates according to

$$k(F) = k_0 \exp\left[\frac{Fx^{ts}}{k_B T}\right],$$

where x^{ts} is the distance between the ground state and transition state along the reaction coordinate. This simple expression assumes that the linear distance to the transition state approximates the reaction coordinate, that k depends on the instantaneous force, and that k_0 and x^{ts} embed features of the intermolecular potential.

More recent theoretical models account for stochastic bond failure under a time-varying force. They also address the bond rupture statistics and link rupture forces with bond chemistry. Evans and Ritchie predicted how applied force increases the bond rupture probability under a dynamically changing force $F(t)$ (24). Using the Bell equation to account for the effect of force on kinetics and an assumption that x^{ts} is independent of force, they derived a convenient, compact relationship between the most probable rupture force F_{mp} (mode of the distribution of rupture forces), the experimental pulling rate, and the parameters k_0 and x^{ts} (24). For a linkage confined by a single barrier, peaks in histograms of rupture forces exhibit a single maximum at the most probable

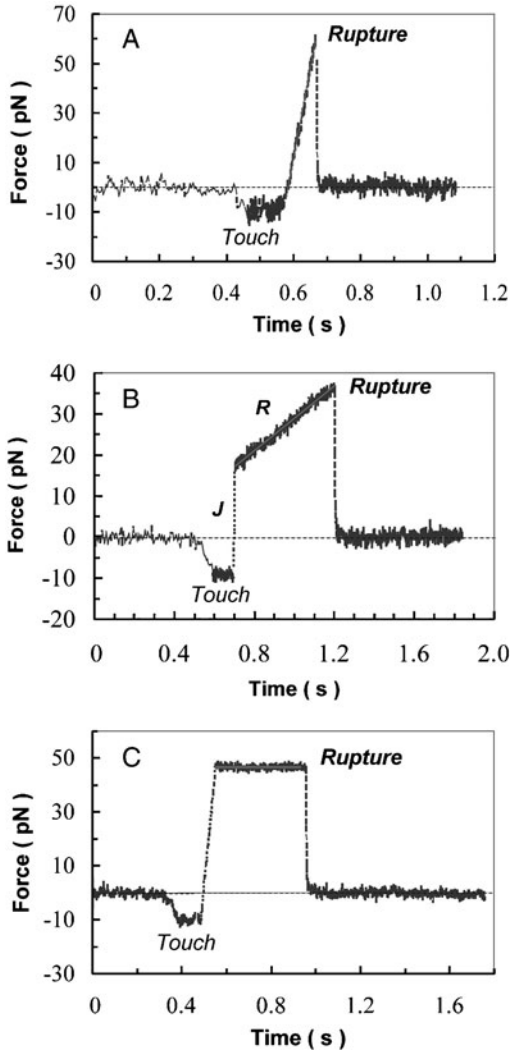

Figure 2

Force-time histories of the rupture of single molecular linkages. (*A*) In steady ramp measurements, after the initial contact the force on the bond increases at a constant rate, d*F*/d*t*, until rupture. (*B*) In jump-ramp measurements, an initial force jump J is followed by a steady force ramp R until bond rupture. (*C*) In the force clamp approach, the force is stepped to a specified value and held until bond rupture. The duration of the level plateau is the bond lifetime at the constant force (50 pN in this case).

rupture force F_{mp}, which is related to the pulling rate r_F by

$$F_{mp} = \frac{k_B T}{x_\beta} ln\left(\frac{x_\beta \times r_F}{k_B T \times k_0}\right).$$

Here k_B is Boltzmann's constant and T is the absolute temperature. The parameter $x_\beta = x^{ts} \cdot F = x^{ts} \cos\theta$ accounts for the fact that the direction of the force may not be collinear with the reaction coordinate. Linear plots of F_{mp} versus log (r_F), which are popularly referred to as dynamic force spectra, can be used to extract values of x_β and k_0 from the slope and x-intercept, respectively.

The activation free energy ΔG^{ts} can be estimated from k_0, where

$$k_0 = \phi \exp\left[-\frac{\Delta G^{ts}}{k_B T}\right],$$

Dynamic force spectroscopy (DFS): measurements of the most probable rupture force versus the $\log_{10}$ of the pulling rate r_F

if one assumes an attempt frequency ϕ (24). I refer to this as the dynamic force spectroscopy (DFS) model.

When there are multiple barriers along the reaction coordinate, the DFS model predicts a stepped force spectrum, which is marked by a sequence of intersecting linear regions with different slopes and x-intercepts. Whereas many force spectra are linear over a range of pulling speeds, others exhibit steeper slopes at high pulling rates. The DFS model attributes these transitions to the emergence of inner barriers nearer the ground state (smaller x^{ts}) at faster pulling rates.

To address some assumptions in the DFS model and the nonlinearities in some force spectra, Szabo, Hummer, and Dudko developed a more general approach, SHD (25–27). Two differences from the DFS model are (*a*) allowing the position of the transition state to vary with force and (*b*) using Kramer's expression for the rate constant. The former is consistent with the Hammond postulate that the ground state and transition states merge as the activation barrier vanishes. The SHD expression for the dependency of the mean rupture force on the pulling rate depends on x^{ts}, k_0, and ΔG^{ts} according to

$$\langle F \rangle \cong \frac{\Delta G^{ts}}{\nu x^{ts}} \left\{1 - \left[\frac{1}{\Delta G^{ts}}\right] \ln \frac{k_0 e^{\Delta G^{ts} + \gamma}}{x^{ts} K V}\right\}.$$

Here K is the probe spring constant, V is the spring velocity, ν is a constant related to the potential, and $\gamma = 0.577$ is the Euler-Macheroni constant. In this model, ΔG^{ts} and k_0 are explicit variables obtainable from data fits to plots of the average force $\langle F \rangle$ versus $\log(r_F)$. The potential-dependent constant ν suggests that the fitted parameters will be model dependent, but the cubic-linear potential ($\nu = 2/3$) appears to be a relatively general model for intermolecular potentials (28). The DFS model is a special case of this more general framework.

The SHD approach predicts that, at intermediate pulling speeds comparable with experimental rates, the average force increases nonlinearly with the logarithm of the pulling rate. This predicted curvature may account, in some cases, for the apparent increase in the slopes of some force spectra at high pulling speeds, without invoking additional activation barriers along the reaction coordinate.

An alternative to steady ramp measurements is the measurement of bond lifetimes under constant force (**Figure 2*C***). In these force clamp measurements, the force is stepped to a constant value, and the bond persistence under this force is the bond lifetime (**Figure 2*C***). Both microscopic models predict dependences of bond lifetimes on the constant force. According to the DFS formalism, for bonds confined by a single barrier, the lifetime ($=1/k_0$) under constant force is

$$\tau(F) = \tau_0 \exp\left[-\frac{F x^{ts}}{k_B T}\right],$$

where τ_0 is the intrinsic, unstressed bond lifetime. The bond survival probability decays exponentially with time, with a decay constant determined by the lifetime at constant force F:

$$P(t) = A \exp\left(-\frac{t}{\tau(F)}\right).$$

For a receptor-ligand tether formed by any of n possible bonds,

$$P(t) = \sum_n A_i e^{-\frac{t}{\tau_i}},$$

where A_i is the formation frequency and τ_i is the lifetime of the ith bound state under a constant force F (29) such that the number of exponentials needed to fit the data is the number of independent bonds with rupture forces above the applied force (29). Extrapolating a set of lifetimes measured at different forces gives the intrinsic lifetime at zero applied force.

Alternatively, the SHD model for a 1D free energy profile predicts that the lifetime depends on force according to

$$\tau(F) = \tau_0 \left(1 - \frac{\nu F x^{ts}}{\Delta G^{ts}}\right)^{1-1/\nu} \exp\left[-\frac{\Delta G^{ts}}{k_B T}(1 - (1 - \nu F x^{ts}/\Delta G^{ts})^{1/\nu})\right]$$

(25). Again, ν depends on the potential and is 2/3 for a linear-cubic potential and 1 for Bell's model. The parameters τ_0, x^{ts}, and ΔG^{ts} are obtained from nonlinear least squares fits of this equation to the lifetimes obtained at different (constant) forces.

A third force-time sequence is the jump-ramp (30), which is not addressed explicitly by the different theories. Here, an initial force jump to a low preset value is followed by a steady ramp (**Figure 2*B***). The preset force can rupture bonds weaker than itself, allowing dynamic characterization of the surviving bonds (29, 30). Alternatively, the initial force jump may trigger a conformational change such that the subsequent force ramp interrogates the mechanical response of a second, force-dependent conformational state (31).

BFP: biomembrane force probe

AFM: atomic force microscope

3.2. Bond Rupture Forces Versus Solution Binding Measurements

It is often assumed that binding affinity is synonymous with adhesion strength and that the force used to rupture adhesive bonds does not alter the unbinding trajectory. However, Socci et al. (32) pointed out that temperature and bond energy, for example, are scalars and are rotationally invariant, whereas force is a vector. Directional forces can bias unbinding trajectories and suppress alternative paths that might otherwise contribute to unconstrained, thermally driven dissociation in solution. This could generate discrepancies between the free energies of bonds obtained from solution binding affinities and adhesion energies. Binding pockets may spatially constrain the ligand reaction coordinate such that thermally activated and force-driven dissociation follow similar paths, but this is not always the case (see Section 4.3).

Theoretical calculations investigated conditions in which affinity correlates with adhesion owing to multiple bonds in parallel, such as those between two parallel cell surfaces (33, 34). Brownian dynamics simulations and deterministic rate equations were used to compute the detachment (adhesive) force between two parallel surfaces separated at constant velocity (33). Below a critical velocity determined by the intrinsic relaxation time of the adhesive bonds, the receptors and ligands are in dynamic equilibrium, and the adhesion increases with the binding free energy ΔG—obtained from the logarithm of the affinity. However, at separation rates faster than the critical velocity, the system deviates from equilibrium, and the adhesion scales with the activation energy for unbinding, ΔG^{ts}. Thus, adhesion via multiple, parallel bonds scales with affinity only at relatively slow pulling rates. The challenge in equating adhesion with affinity is suggested by the slightly better correlation between CD2/CD58 adhesion energies and the logarithm of the dissociation rates (G^{ts}) than between CD2/CD58 and the logarithm of the affinities (G_{eq}) (21).

3.3. Single Bond Rupture Measurements: Methods

The two main instruments used to quantify single, noncovalent protein bond strengths are the biomembrane force probe (BFP) and the atomic force microscope (AFM). The BFP quantifies the rupture of individual protein bonds by using a soft red blood cell (RBC) as the force transducer

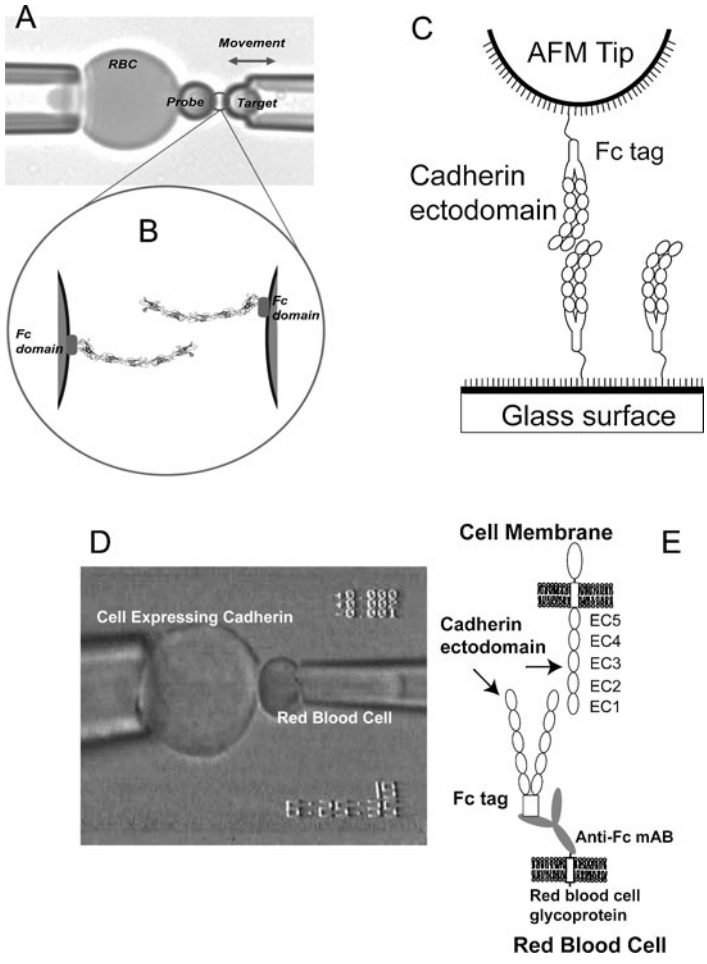

Figure 3

Sensitive force measurement instruments for quantifying the strengths and kinetics of noncovalent receptor-ligand bonds. (*A*) In the biomembrane force probe, a cadherin-modified microbead is bound to the surface of a red blood cell (RBC), which is aspirated into the pipette (*left*). The opposed micropipette holds a second bead modified with cadherin fragments (*right*). (*B*) Illustration of the Fc-tagged cadherin ectodomains immobilized on the two beads. (*C*) Schematic of an atomic force microscope (AFM) tip modified with a receptor (Fc-tagged cadherin ectodomain) and a substrate modified with the target ligand (Fc-tagged cadherin ectodomain). The proteins are tethered to the surfaces via flexible spacers. (*D*) Micropipette manipulation instrument showing a test cell expressing the cadherin receptor (*left*) and an RBC modified with ligands (*right*). The test cell is aspirated into a glass pipette. The RBC is aspirated into an opposed pipette. (*E*) Schematic illustrating the protein configurations on the opposing cells in the micropipette experiment. The C-cadherin on the test cell membrane (*top*) faces the Fc-tagged cadherin ectodomain, which is composed of extracellular domains (ECs) 1–5. The latter is bound to the RBC surface (*bottom*) via a monoclonal anti–human Fc antibody (anti–Fc mAb), which is covalently bound to the RBC.

(35). In the BFP setup (**Figure 3*A***), an RBC is aspirated into a pipette. A microbead modified with immobilized ligands is "glued" biochemically onto the RBC. The opposed micropipette holds a cell or a second bead coated with the complementary receptor (**Figure 3*B***). Both beads (*left*) and target surface (*right*) (**Figure 3*A***) are sparsely modified with receptors and ligands to increase the likelihood that binding events reflect single biomolecular linkages. The two probes are brought

into contact and pulled apart with a defined force-time trajectory. At bond failure, the RBC recoils back to its unperturbed shape, and the RBC distortion at failure determines the rupture force. F_{mp} is then determined from histograms of the rupture forces measured at loading rates r_F from 10–10^6 pN s^{-1}. Dissociation rates are extracted from data fits to one of the models described in Section 3.1.

The AFM (**Figure 3*C***) is also commonly used to extract rate constants from single bond rupture measurements. In this case, a silicon nitride probe tip is modified with an immobilized receptor (**Figure 3*C***) (36–38). The target surface with complementary ligands can be either a second model surface modified with target ligands or a cell membrane. The challenges of data acquisition and interpretation depend on whether the proteins are anchored to a rigid substrate or to a soft membrane (39, 40). As in BFP measurements, the receptor-ligand bonds can be pulled with any of the force-time trajectories in **Figure 2**. The following examples illustrate how single bond rupture, using different force-time trajectories, can extract biophysical and mechanistic details of cell adhesion molecule function.

3.4. Measured Strengths of Single Molecular Linkages: Chemistry and Mechanism

In addition to extracting dissociation rates, single bond rupture studies can also reveal mechanistic details, such as the existence of multiple binding interactions or force-actuated changes in unbinding pathways. Receptor-ligand bonds in series with cytoskeletal linkages can also probe cytoskeletal connections or inside-out signaling (Section 3.4.3). There is a vast literature on single molecule measurements of forced macromolecular unbinding and unfolding (41–43). This review focuses on nanomechanical studies of adhesion molecules that reveal novel aspects of their mechanical functions.

3.4.1. Selectins and catch bonds. Single bond rupture studies of selectin bonds with glycoprotein ligands illustrate several important aspects of forced receptor-ligand bond rupture. First, unique force-lifetime signatures determined by subjecting bonds to different force histories has identified a class of linkages referred to as catch bonds. Second, comparisons of bond parameters obtained with different rupture protocols demonstrate that measurement outcomes can depend on the force history. Third, both results illustrate the potential limitations of interpreting bond rupture data in terms of 1D reaction coordinates.

Selectins expressed on the vascular endothelium at sites of inflammation capture neutrophils by binding to glycoprotein ligands on neutrophil surfaces. Once the bonds are formed, these tethers experience nearly instantaneous loading relative to the timescale of bond relaxation. The bond formation rates and lifetimes under different fluid flow govern neutrophil rolling at different fluid shear stress and ligand densities.

Measurements of selectin-glycoprotein bond rupture, carried out in steady pulling, constant force, and jump-ramp modes (**Figure 2**) (31, 44–51), have identified mechanically distinct adhesive states. However, the manifestation of these different bond properties and their influence on the lifetimes and strengths of the stressed bonds depends on the force-time history.

The lifetimes of P-selectin/P-selectin-glycoprotein-ligand-1 (PSGL-1) bonds subject to constant force reveal that, in contrast to the Bell prediction, the lifetime does not always decrease with force. Initial shear flow studies of neutrophil rolling did indeed verify Bell's prediction that force accelerates bond dissociation (23, 45). Subsequent AFM measurements of the same system explored bond lifetimes over a wider range of forces and showed that, whereas the lifetime decreases with forces >25 pN, at forces <25 pN, the lifetime actually increases with increasing force (31).

Slip bond: a noncovalent receptor-ligand bond whose lifetime decreases with the magnitude of the force applied to the bond

This counterintuitive increase in lifetime with applied force is the functional signature of catch bonds. Dembo and coworkers first predicted the existence of catch bonds (52), but demonstration of a bona fide catch bond requires demonstrating this unusual force-lifetime relationship—a challenge that eluded investigators for several years. Marshall et al. (44) first clearly demonstrated catch bond behavior with P-selectin.

A combination of single bond rupture and flow assays quantified increases in the P-selectin/PSGL-1 bond lifetimes over a range of constant applied forces (44). Force clamp measurements (**Figure 2*C***) determined the lifetimes of bonds subject to a range of (constant) forces. The P-selectin bond lifetimes first increased with force up to an optimum value that depended on the oligomerization state of the PSGL-1 molecules, e.g., dimers versus monomers. Beyond the force optimum, the lifetimes then decreased exponentially with the applied (constant) force—a characteristic of the slip bond behavior reported by Alon et al. (45). Thus, P-selectin bonds exhibit catch-slip behavior.

Leukocytes require a threshold shear stress to form persistent tethers and roll on the vascular endothelium. This suggested the existence of catch bonds (53). In shear flow assays, which are described extensively elsewhere (54), bond loading is analogous to force clamp measurements because the bonds experience nearly instant loading upon tether formation, followed by a constant stress determined by the flow rate. The force clamp closely mimics the force history of cell-surface bonds in flow. Indeed, in recent years, flow assays have been used to identify and characterize proteins exhibiting catch bond behavior. Examples include enteric bacterial protein FimH (55, 56), von Willebrand factor (8), and integrins (57). Several reviews describe this rapidly expanding field (31, 58–61).

Jump-ramp measurements verified that a critical force is required to mechanically switch the adhesive state of selectin, and quantified the force threshold (47). Under a steady ramp (**Figure 2*A***), the P-selectin bonds had no apparent strength at slow pulling speeds, but after an initial abrupt jump to ~30 pN, the bond strength increased with loading rates as slow as 35 pN s^{-1}. Varying the amplitude of the force jump showed that an initial 30-pN jump was sufficient to switch P-selectin to an adhesive state capable of resisting dynamically increasing forces.

Under a steady force ramp, most protein bonds exhibit finite strengths that increase with the logarithm of the pulling rate. However, the P-selectin/PSGL-1 bond had no strength at slow, constant pulling speeds (46). This persisted at pulling rates up to ~300 pN s^{-1}. At ~200 pN s^{-1}, the emergence of a second peak in the histogram at a finite (nonzero) rupture force coincided with the diminution of the peak at zero force, which suggests that the applied force activates the formation of a stronger bound state above a threshold pulling speed. These steady ramp results are, therefore, also consistent with catch bond behavior.

The three force-time sequences (**Figure 2**) identified different dynamic response signatures of P-selectin/PSGL-1 catch bonds. Nevertheless, the bond lifetimes determined with these three methods differed, even though the same receptor-ligand pairs were used. Values also differed from lifetimes measured in shear flow assays. These discrepancies had been attributed to experimental variables such as protein origin, measurement techniques, and analysis methods. A rigorous comparison of the different approaches, using the same proteins, showed that the different force-time histories used underlie the differences in extracted bond parameters (31).

The dependency of bond lifetimes (or dissociation rates) on the force history (see **Figure 2**) might be expected because kinetic processes are nonequilibrium and therefore path-dependent. However, prior data analyses were based on several assumptions, the most significant being that the kinetic rates were single-valued functions of the instantaneous force. Recent studies demonstrate that this is not the case (31). The assumed first-order dissociation along a single reaction path may also be overly simplistic, as in the case of catch bonds. These results highlight the need to

develop a more general theoretical framework that describes the interplay between force and the complexities of biomolecular bonds.

The properties of catch bonds revealed by nanomechanical measurements identified force-dependent dissociation mechanisms that define the biological functions of these proteins. The inability of solution binding measurements to reveal these details emphasizes the need for sensitive nanomechanical tools to determine the mechanisms of adhesion protein functions.

A molecular explanation for catch bond behavior, which can be accounted for phenomenologically if $x^{ts} < 0$ in Bell's rate expression, involves force-actuated switching between two conformational states that have different unbinding reaction coordinates (4, 47, 61–64). For catch-slip bonds, below the force optimum, increasing the applied force biases the conformation toward the pathway with the higher barrier such that the lifetime increases with force.

Interestingly, a common structural motif of the catch-bond proteins investigated thus far appears to involve auto-inhibition that is released by force to activate a strong binding state. Both P-selectin and FimH exhibit high-affinity and low-affinity states whose interconversion correlates with the opening and closing of a hinge region. In FimH, the hinge angle appears to control binding between the active site and an inhibitory site on the same molecule (65, 66), whereas the hinge opening in P- and L-selectin corresponds with a structural change in the binding site that enhances the affinity (67, 68). Mutagenesis studies in conjunction with force measurements appear to support these proposed mechanisms (56, 65, 67–69).

Modular binding: binding between proteins that consist of multiple domains in which more than one domain module can bind to another, similar protein

Ectodomain: the segment of a membrane-bound protein that is on the outside of the cell

ECs: cadherin β-barrel extracellular domains, numbered 1–5, that are core building blocks of the full-length cadherin ectodomain

3.4.2. Multidomain adhesion molecules and modular binding mechanisms. The structures of many cell adhesion proteins are modular, composed of multiple, tandem repeats of structurally similar domains (70, 71). Some of these proteins not only bind identical proteins (homophilic bonds) on an opposing cell but also associate with similar proteins on the same membrane. These adhesive and lateral bonds could involve the same or different structural modules, and this complexity creates particular challenges for identifying functional interactions and their role in cell adhesion. Identification of different protein binding interactions and the participating domains is needed to define the molecular mechanisms of adhesion and to identify minimal functional units, which could be used in tissue engineering scaffolds, for example.

Cadherins are intercellular adhesion molecules whose adhesive ectodomains consist of multiple, tandem repeats of ~4.5-nm β barrel extracellular domains (ECs), which are numbered 1 through 5, with calcium bridges between adjacent EC segments (**Figure 4*A*,*B***). Several studies indicate that cadherins on adjacent cells adhere via their N-terminal domains in a complex formed when the tryptophan at position 2 (W2) from each protein inserts into a hydrophobic pocket on the opposing EC1 domain (**Figure 4*C***). Cadherins are also postulated to interact laterally to enhance binding avidity (72, 73). Adhesion between EC1 domains is supported by structural data, but other functional domain interactions have not been conclusively identified in crystal structures. Single bond rupture measurements were used to identify different cadherin binding states, characterize their properties, and map them to structural regions of the protein.

The more than 20 members of the type I classical cadherin subfamily are named according to the tissues from which they were first isolated. Single bond rupture measurements were performed with ectodomain fragments of epithelial (E-) cadherin, neural (N-) cadherin, and *Xenopus* cleavage stage (C-) cadherin. The following describes the use of cadherin mutants and force-time sequences to identify multiple, independent bonds between these proteins and to map the bonds to different structural regions (29, 30, 36, 74).

The force histograms measured with full-length C-cadherin ectodomains (CEC1–5; **Figure 5*B***) are very broad with a prominent peak at ~45 pN (*blue curve*, **Figure 5*A***). DFS analysis of the prominent peak (**Figure 5*B***) determined that the dissociation rate for this bond is

slow, on the order of 10^{-5} s^{-1} (29). E-cadherin and C-cadherin exhibit similar broad histograms with the same qualitative features (29, 30).

Multidomain protein: In this review, multidomain proteins are large proteins whose extracellular domain structures consist of multiple, tandemly arranged, independently folding domains.

The force distributions measured with the full-length cadherin ectodomains were too broad to attribute to a single interprotein bond, thus more extensive analyses of the force distributions were necessary. Deconvolution of the force histograms into different cadherin binding interactions used cadherin domain deletion mutants as well as three different force-time trajectories (**Figure 2**) (29, 30). These approaches together revealed that opposing full-length ectodomains form multiple bound states with different strengths and kinetics that map to different structural regions of the protein.

Histograms obtained with EC12 fragments lacking domains 3–5 are by contrast much simpler, as they exhibit a narrower, major peak (*green curve*, **Figure 5*C***). Analyses of the linear force spectrum of this major peak determined that the EC12/EC12 bond (*a*) is weaker than the prominent bond between the full ectodomains (*blue curve*, **Figure 5*A***) and (*b*) dissociates rapidly with rates of 0.01–0.02 s^{-1} (29, 30). The width of the peak suggested a second "hidden" peak at lower forces (*orange curve*, **Figure 5*C***). The jump-ramp force sequence (**Figure 2*B***) (30) distinguished the different bond populations contributing to the histogram in **Figure 5*C*** according to their dynamic responses to both the jump and subsequent ramp phases. An initial force jump broke bonds with strengths <20 pN, enabling separate analysis of the bound state defined by the green curve in **Figure 5*C***. Bonds rupturing during the jump phase define a very weak bond with a fast dissociation rate of $\sim$4 s^{-1} (*orange curve*), which is consistent with the initial encounter complex detected by single-molecule fluorescence resonance energy transfer measurements (75). Similar analyses of histograms obtained with the full-length ectodomains showed that the same EC12-dependent bonds contribute to the low force region of the histogram (**Figure 5*A***, *orange and green curves*).

More extensive jump-ramp analyses of the histograms obtained with the full-length mouse E-cadherin and C-cadherin ectodomains also identified two strong bonds rupturing at >40 pN (**Figure 5*A***, *blue and red curves*). Domain deletion mutants mapped the strongest bond to EC3. These jump-ramp measurements with cadherin deletion mutants thus identified four distinct binding interactions with different strengths and kinetics that map to different structural regions of the ectodomain. Human E-cadherin exhibits similar behavior (74). The results suggest that domains 1–3 compose the smallest fragment containing all binding interactions characteristic of the full-length protein.

Force clamp measurements (**Figure 2*C***) validated the jump-ramp analyses of the broad cadherin histograms. As discussed in Section 3.1, the time-dependent survival probability of receptor-ligand bonds held by multiple, independent linkages is a superposition of **n** exponential functions. The number of states surviving the jump to the low, constant force determines the number of exponentials and associated lifetimes needed to define the decay profile (29, 30). This approach confirmed that three bonds survive the jump to 40 pN (*green*, *blue*, *and red curves*, **Figure 5*A***). The survival probability curve that was computed with the rate constants determined from the jump-ramp analyses describes the experimentally measured decay curve (29). This example demonstrates the combination of protein engineering and force-time trajectories to deconstruct complex force histograms obtained with multidomain proteins and thereby to identify functional regions of the protein.

Similar methodology was used with NCAM, a multidomain adhesion protein of the immunoglobulin (Ig) superfamily (71). Its ectodomain is composed of five tandemly arranged Ig-type domains followed by two fibronectin type III repeats (seven extracellular modules total). NCAM binds via the immunoglobulin 1–5 segments (Ig1–5) to NCAM on adjacent cells. Solution binding measurements with several different NCAM fragments, as well as differences between crystal structures (76, 77), contributed to conflicting models for both *cis* and *trans*, homophilic NCAM binding.

AFM measurements of the rupture of single NCAM/NCAM bonds also identified two different homophilic bonds that require different structural modules (37). Force histograms exhibited two distinct force peaks, and this distinct functional signature was exploited in subsequent structure/function analyses, which mapped the stronger bond to Ig3 and the weaker bond to the first Ig1 domain (78). These AFM measurements therefore demonstrated that NCAM forms either of two bonds that involve different domains. Although solution binding affinities with different NCAM fragments also supported these findings (79), the bond rupture data demonstrated that these are structurally distinct bonds and quantified their mechanical strengths, dissociation rates, and differences in x^{ts}, which scales the mechanical response to force.

However, because the molecules in AFM measurements are orientationally unconstrained on the probe and tip, it is not possible to establish whether the interactions correspond to *cis* or *trans* bonds on cell surfaces. The bond rupture measurements can nevertheless identify the ability to form different bound states, and the use of different protein mutants can in turn map the homophilic bonds to different structural regions.

3.4.3. Probing adhesion protein links to the cytoskeleton. Sections 3.2–3.3 focus on ectodomains of adhesion proteins, but many cell adhesion proteins are coupled to the cytoskeleton. The mechanical system therefore comprises multiple bonds in series, namely, the cytoskeleton-receptor linkage, membrane anchor, and receptor-ligand bonds (**Figure 6*A***). Inside-out signaling can also regulate intrinsic receptor-ligand bond properties (80). Both the BFP and AFM have been used to probe linkages at soft membrane surfaces (41, 81, 82), but currently only the BFP has sufficient force and distance sensitivity to interrogate receptor-cytoskeletal linkages.

The series of receptor-ligand, membrane, and receptor-cytoskeleton linkages exhibit distinct force signatures that are used to interrogate the different interactions. **Figure 6*B*** shows force-time trajectories measured between a PSGL-1-modified probe and a leukocyte in the absence and presence of the actin-disrupting drug latrunculin A (39). PSGL-1 binds P-selectin, which is anchored to the actin cytoskeleton through its cytodomain. The cytoskeleton-receptor and the receptor-ligand bonds respond to the time-dependent forces. However, upon failure of the receptor-cytoskeleton linkage, continued pulling on the membrane extrudes nanotube tethers as the membrane separates from the cytoskeleton. These tethers can extend up to a few microns. In **Figure 6*B***, the initial slope is characteristic of receptor-ligand bonds under a steady force ramp, but the deviation from the dashed line signals receptor-cytoskeleton bond rupture. Beyond the deviation at ⊗, the force reflects the fluidlike viscous drag of tether extrusion, which continues until PSGL-1 bond rupture. Actin disruption with latrunculin A abolishes the initial linear region of the curve (**Figure 6*B***) attributed to P-selectin/cytoskeleton bonds, such that the curve exhibits only the viscous drag and final PSGL-1/P-selectin bond rupture.

These measurements of cytoskeletal coupling require high-resolution distance and force measurements to unambiguously detect the subtle deviations in the force-time trajectories signifying the different unbinding events. This is possible with the BFP but currently not with the AFM.

4. SURFACE FORCE MEASUREMENTS: DISTANCE-DEPENDENT FORCES AND ADHESION BETWEEN BIOLOGICAL MEMBRANES

4.1. Surface Force Apparatus: Forces Governing Biomolecular Adhesion

In contrast to the nonequilibrium single bond rupture measurements, the SFA quantifies the distance dependency of forces between two surfaces. It is also used to measure near-equilibrium

adhesion energies rather than force. Time-dependent measurements also reveal how conformational dynamics affect force signatures (83). The SFA quantifies the normalized force between two curved surfaces in liquid (or vapor) as a function of their separation distance (**Figure 7*A***) (84, 85). Absolute distances are determined within ± 0.1 nm by interferometry (**Figure 7*B***).

DC-SIGN: dendritic cell-specific integrin-grabbing nonintegrin

The SFA measurements quantify the net force between crossed hemicylinders F_c normalized by the geometric average radius $\langle R \rangle = \sqrt{R_1 R_2}$ of the cylinders. This normalized force F_c/R is directly proportional to the interaction energy per area E_A between equivalent flat plates, according to the Derjaguin approximation: $E_A = F_c/2\pi R$ (86, 87). This relationship is valid when $R \gg D$. Because $R \sim 1$ cm and $D < 100$ nm, SFA measurements yield intersurface energies. The normalized force sensitivity $\Delta F/R$ is $\pm$ 0.1 mJ m^{-2} and enables quantification of weak interactions with energies on the order of k_BT (or 0.6 kcal mol^{-1} at 25°C) (83).

The distance dependency of the intersurface forces reveals structural details of molecules or molecular complexes confined between the surfaces. For example, the dimensions (lengths) of several different proteins measured with the SFA agreed quantitatively with the crystallographic dimensions of the proteins and/or complexes (21, 65, 88–92).

4.2. Conformational Flexibility and Molecular Recognition in Innate Immunity

Surface force apparatus measurements of dendritic cell–specific integrin-grabbing nonintegrin (DC-SIGN), an adhesion protein expressed on dendritic cells in the immune system, identified a binding-dependent conformational change in the protein that is facilitated by flexible linkers in the protein architecture. DC-SIGN recognizes carbohydrate patterns on several different pathogens (93). Most pathogens that bind to DC-SIGN are internalized by the cells and are neutralized, but other pathogens, such as HIV, exploit DC-SIGN to infect cells (94, 95). Knowledge of design rules for pathogen recognition could be used to design therapeutic agents that block pathogen infectivity.

DC-SIGN is a tetramer of single polypeptide chains, and the folded structure is composed of an α-helical, coiled-coil neck that is terminated by four clustered carbohydrate recognition domains (CRDs) (**Figure 7*C***) (96). Because the individual CRD-glycan affinities are low, the neck is thought to direct the CRDs toward the pathogen and away from the cell surface at the same time that the terminal CRD clustering enhances the ligand-binding avidity.

Force-distance profiles measured between membrane-anchored, oriented DC-SIGN ectodomains and bilayers displaying glycan ligands (**Figure 8*A***) identified key molecular features that contribute to DC-SIGN recognition and adhesion (97). By quantifying the DC-SIGN dimensions and the adhesion energy, SFA measurements identified a binding-dependent conformational change that enhances adhesion between DC-SIGN and surface-bound ligands.

Two findings indicate that DC-SIGN undergoes a binding-dependent conformational change: (*a*) the measured range of the steric repulsion between DC-SIGN monolayers and membranes without glycolipid versus glycolipid-displaying bilayers and (*b*) the dynamic jump to contact between protein and glycolipid monolayers. In control measurements between DC-SIGN and bare lipid membranes (**Figure 8*A***), the onset of the repulsive force at D_{Rep} corresponds to the protein thickness. The steep increase in repulsion at $D < D_{Rep}$ demonstrates that the neck is rigid. The protein did not adhere to the bare membranes. From the range of the repulsion D_{Rep}, the measured neck thickness (length) is 28 nm, after accounting for the thickness of the CRD region. This is the first direct measurement of the neck length and the first demonstration that the relatively rigid neck holds the CRDs away from the membrane (**Figure 8*B***).

In contrast, with glycolipid on the target membrane (see **Figure 7*C***), the DC-SIGN monolayer spontaneously jumped into contact with the glyolipid-coated membrane (**Figure 8*A***). The surfaces came to rest at an equilibrium distance D_{Eq} that is smaller than the range of the steric repulsion D_{Rep} in the absence of ligand (**Figure 8*A***). In SFA measurements, jumps into contact occur from distances at which the gradient in the intersurface potential exceeds the spring constant. The difference between the equilibrium thicknesses of DC-SIGN in the absence and presence of glycan indicates that the protein undergoes a binding-dependent conformational change (**Figure 8*B***). The magnitude of the conformational change increases with the glycan surface density and hence with the adhesion, up to a limiting value of 4.8 nm (97).

This conformational change is attributed to flexibility in the linkers between the CRDs and neck that enable the CRDs to rearrange and optimize ligand engagement. Although crystal structures suggested flexibility in the linker region, the SFA measurements directly demonstrated the consequences of this flexibility for DC-SIGN recognition. This flexibility and CRD adaptability to ligand distributions is thought to be important because it may enable DC-SIGN to recognize a broader range of pathogens than proteins in which the CRDs are more rigidly aligned (97).

4.3. Tethered Ligands

Surface force measurements between ligands (biotin) tethered to polymers and membrane-immobilized streptavidin demonstrated the impact of flexible tethers on the receptor-ligand interaction potential (**Figure 9*A***). Force-distance profiles between streptavidin and flexibly tethered biotin monolayers demonstrated that the efficiency of strong intersurface binding is determined by the frequency of rare polymer (tether) fluctuations, the tether length, and the receptor-ligand bond energy. The most obvious effect of ligand tethering is the increased range of intersurface binding. In force curves between streptavidin monolayers and biotin bound to a 0.4–1-nm tether, there is no apparent attractive force between the two surfaces at membrane separations >1 nm (**Figure 9*B***, *solid line*). However, when biotin is tethered to flexible polymers, the binding distance from which the surfaces jump into contact is 15 nm (*point b*, **Figure 9*B***). The surfaces come to rest at a final separation D_{Eq} (*point c*, **Figure 9*B***) determined by the balance between the osmotic repulsion by the polymers and the receptor-ligand attraction. Importantly, the polymer increases the range of the attractive intersurface potential from ~1 nm, in the case of membrane-bound biotin, to nearly the fully extended end-to-end tether length of the chain $L_c = \mathbf{a}N$. Here N is the polymerization index and **a** is the monomer length. On average, the tethered biotins should reside at $\sim 0.57L_c$, and large excursions from this average are rare. The surprising result was that the tethers increased the binding distance to nearly the full length of the chain. Accordingly, the binding distances d_B increase with N (98), as do the final equilibrium separation distances D_{Eq}.

From analyses of the force-distance curves as a function of the degree of polymerization N and of the receptor-ligand bond energy, Wong & Kuhl (98) constructed an energy-state diagram depicting binding distances in terms of the energetics of polymer extension versus the receptor-ligand potential. This state diagram predicts points of instability where the receptor-ligand bond energy balances the chain extension energy. It also predicts points of binding or de-adhesion, depending on whether the surfaces are approaching or separating, respectively.

The binding dynamics are also fundamentally linked to chain fluctuation timescales. Initial analyses of the force-distance profiles showed that the binding distance depends on the frequency of rare, large excursions from the average position of the chain ends. This was confirmed by theoretical modeling (100). For example, the typical exploration time at a distance D from a chain

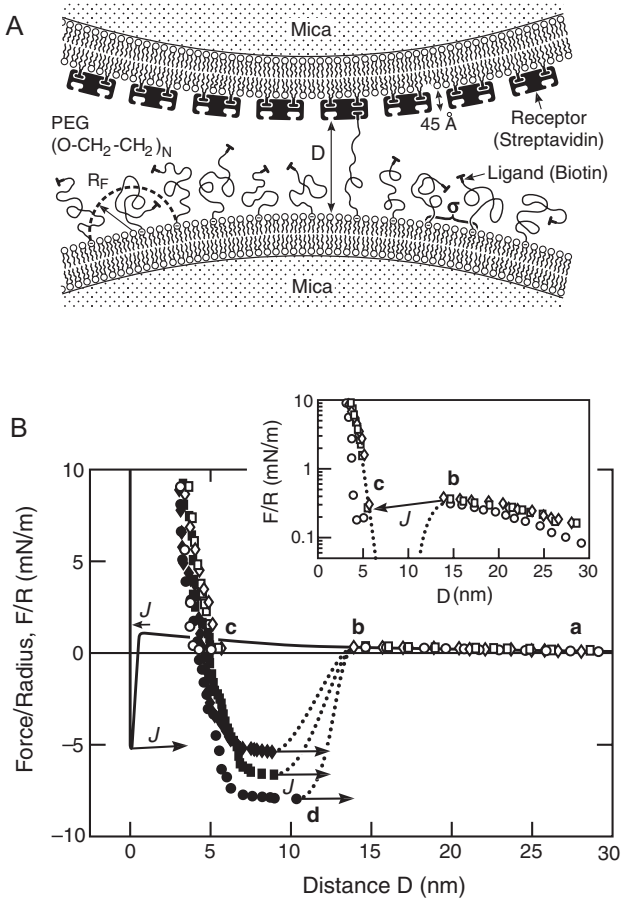

Figure 9

(*A*) Schematic of the polyethylene glycol tethered biotin (PEG-biotin) and streptavidin configurations in the surface force apparatus measurement. The polymer molecular weight is 2000. Here D is the distance from the outer edge of the streptavidin layer to the outer lipid head group surface on the opposing surface, and R_F is the Flory radius of the PEG chain. (*B*) Interaction force profile as a function of separation distance between streptavidin and PEG-biotin normalized by the radius of curvature, R. The solid curve shows the interaction between streptavidin and 5-mol% biotin-lipid without the PEG tether. Open symbols show forces measured during approach and black symbols, during separation. The different sets of data correspond to the first approach (*open circles*) and separation (*black circles*), second approach (*open squares*) and separation (*black squares*), and third approach (*open diamonds*) and separation (*black diamonds*). Arrows (*J*) denote jumps into contact and jumps out of contact. The binding distance is the separation (*b*) from which the surfaces jump into contact at the equilibrium separation (*c*). The distances from which the surfaces pull out of contact (maximum adhesion) are indicated by right-pointing arrows (*d*). Reproduced with permission from (99).

anchor would be

$$\tau = \tau_0 \exp\left(\frac{E_{ext}(D)}{k_B T}\right),$$

where τ_0 is the intrinsic relaxation time of a single chain, or the Zimm time, or

$$\tau_0 \approx \frac{\eta R_F^3}{k_B T}.$$

Here $E_{ext}(D)$ is the extension energy at D, η is the viscosity, and R_F is the Flory radius of the chain. Assuming a parabolic potential for the polymer extension,

$$E_{ext}(D) = \frac{(D/R_F)^2 k_B T}{2}.$$

Tethered ligands: ligands that are connected to the supporting surface via long molecular linkers (tethers). Tethers can be flexible or rigid.

Thus, the typical exploration time for the free end of a 2000-MW chain near the fully extended length of 16 nm is ~1 ms, which is well within the measurement timescale of seconds to minutes. These high-resolution, force-distance measurements together with theoretical calculations demonstrate that polymer fluctuation dynamics and receptor-ligand bond energy determine the binding efficiency of tethered ligands. They further define design rules for enhancing drug targeting or cell capture with tethered ligands. As a practical example of the impact of tethering, microparticles decorated with tethered ligands appear to exhibit higher affinity for vascular endothelial cells in blood flow than for microparticles with ligands modified without tethers (101).

4.4. Multidomain Proteins and Modular Binding Interactions

SFA measurements also identified novel interactions between multidomain, homophilic adhesion molecules. AFM measurements can identify adhesive states formed by NCAM and cadherins (Section 3.4.2), but they give no information about the structures of the complexes corresponding to the bound states. SFA measurements of the same proteins provide spatial details and force-distance signatures that have identified distinct structural regions required for binding interactions. As in the AFM studies, the quantitative impact of deleting domains on the force-distance signatures demonstrated that NCAM and cadherins form multiple, spatially distinct bound states that require different regions of the ectodomains.

The normalized force or energy/area as a function of the bilayer separation was measured between oriented cadherin monolayers immobilized on supported lipid bilayers (see **Figure 7*B***). During approach, the cadherin monolayers repel ($F > 0$) at $D < 55$ nm, but upon separation, they adhere at three distinct membrane gap distances: 39 nm, 53 nm, and 44 nm (**Figure 10*A***). The method used to detect these discrete adhesive minima is described elsewhere (102, 103). The adhesion energies at the different distances also decreased in the order 39 nm >53 nm >45 nm (**Figure 10*A***).

The force-distance profiles and adhesive minima were interpreted in terms of the cadherin structure by comparing the distances of adhesive minima to the extended length of the cadherin ectodomain and accounting for the dimensions of the anchoring layers and for possible cadherin configurations compatible with the distances. Structure-function analyses based on the impact of EC domain deletion mutants on the force-distance signature (**Figure 10*A***) mapped adhesion at 53 nm to EC1/EC1 binding (**Figure 10*B***), but the stronger bond at 39 nm requires EC3 (see **Figures 4*C*** and **10*B***) (104). Allowing for the possibility that cadherins could form both *cis* and *trans* bonds, any of the models in **Figures 10*C*** and **10*D*** could account for adhesion at the membrane distance of 39 nm.

SFA measurements similarly demonstrated that NCAM forms two spatially separated bound states that require different domains (79). Consistent with the AFM data, the weak and strong bonds map to the first and third domains, respectively. The SFA measurements with NCAM also ruled out binding interactions proposed on the basis of some crystal structures.

The flexibility of both cadherin and NCAM and their ability to bind identical proteins on an opposing cell and on the same membrane prevents the unambiguous attribution of these bound states to lateral or to adhesive interactions. Additional information is needed to determine how these different binding interactions influence NCAM function on cell membranes. With cadherins,

kinetic signatures (see Section 5.2, below) provided the needed data to begin to distinguish between the different interpretations in **Figures 10*C*** and **10*D***.

MP: micropipette manipulation technique

5. CELL BINDING KINETICS TEST MECHANISMS OF PROTEIN-MEDIATED INTERCELLULAR ADHESION

5.1 Micropipette Manipulation Measurements of Cell Binding Kinetics

Kinetic measurements of intercellular binding are used to develop and test mechanistic models of protein-mediated cell adhesion and to quantify relevant rate constants and 2D affinities, when feasible, for kinetic steps in the reaction pathway (105). This is analogous to studies of enzyme reaction mechanisms in which comparisons of measured reaction time courses with kinetic model predictions identify mechanisms underlying chemical conversions.

Micropipette manipulation (MP) measurements quantify the kinetics and 2D affinities of protein-mediated cell binding (106). In this instrument, two cells held by opposing micropipettes are brought into contact for a defined period and then separated (**Figure 3*D***) (107). Kinetic measurements (106) quantify the time evolution of the cell binding probability $P(t)$, which is the ratio of the number of binding events n_{adh} to the total number N_{total} of cell–cell contacts, $P(t) = n_{adh}/N_{total}$. The rate of change of $P(t)$ reflects kinetic pathways and associated 2D affinities and kinetic rates of the binding reactions (106). Typically, one of the cells is an RBC, and the second cell expresses the adhesion molecule of interest (**Figure 3*D***). Cell adhesion causes the RBC to distort during separation, and it recoils to its unperturbed shape at bond rupture. This approach was used extensively to study the binding kinetics of *Fcγ* receptors, selectins, integrins, and CD8 with their respective receptors (106, 108–113). In contrast to bond rupture measurements, measured binding affinities are independent of the amount of force needed to break the bonds. MP is also used to quantify cell adhesion (114) but is not considered here.

5.2. Cadherin-Mediated Intercellular Binding Kinetics

The model of cadherin-mediated adhesion, popularized by the structure of the ectodomain and of ectodomain fragments (**Figure 4*C***) (115), involves simple cadherin association via the binding mechanism $A + A \rightarrow A_2$, where A is monomeric cadherin and A_2 is the *trans* EC1–EC1 complex. The probabilistic rate equation for this mechanism describes a single exponential rise in the binding probability $P(t)$ to a limiting plateau (**Figure 11*A***).

Kinetic measurements were done with Chinese hamster ovary cells engineered to express the full-length cadherin and with RBCs modified with immobilized, recombinant cadherin ectodomains (**Figure 3*E***). In contrast to the structure-based model (**Figure 11*A***), the binding kinetics exhibit an initial, fast increase in the binding probability to a first plateau at $P(t) \sim 0.4$–0.5, followed by a 2–5-s lag and a second plateau at a higher binding probability $P_2 \sim 0.8$ (**Figure 11*B***). This additional complexity is not captured by the simple mechanism in **Figure 4*C***.

This distinct kinetic fingerprint was exploited in structure-function analyses of cadherins. Studies with mutants lacking the transmembrane and cytoplasmic domains, EC3 domain, or EC3–5 mapped the two-stage kinetics to the ectodomain (105). The first, fast step requires the first domain EC1, and the lag phase and rise to the second plateau P_2 requires the third domain EC3.

Fitting the kinetic data to different models showed that the simple model $A + A \rightarrow A_2$ describes the first binding step but not the second stage. Comparisons with kinetic models instead suggest that the second binding step, which requires EC3, may involve cadherin oligomerization (D. Leckband, unpublished observations). The kinetic data was thus key to identifying the functional contributions of the different binding interactions to intercellular adhesion.

Together, these kinetic, AFM, and SFA measurements constitute a complementary, self-consistent set of data that has identified multiple cadherin binding interactions and their roles in the assembly of intercellular junctions.

5.3. Tethers Enhance Intercellular Binding Kinetics

MP measurements also assessed the effect of receptor tethering on intercellular binding kinetics. The long, anchoring tethers of many cell surface glycoproteins are postulated to increase binding to target ligands either in solution or on cells. Kinetic measurements quantitatively tested this hypothesis.

P-selectins are long, cell-surface glycoproteins with binding sites at the ends of tethers that are composed of nine consensus repeats (CRs) that extend ~27 nm from the cell membrane. E-selectin contains six CRs. To determine the impact of the receptor lengths on binding kinetics, Huang et al. (116) used two different recombinant P-selectin constructs. The soluble P-selectin (sP) comprises the LecEGF (lectin-epidermal growth factor) region and nine CRs, whereas the sPE construct consists of the LecEGF domain and a C-terminal epitope tag but lacks CRs. The different proteins were bound to the RBCs via antibodies such that sP was bound at the fourth consensus repeat from the membrane whereas sPE was bound via the epitope tag. Thus, sP extended beyond the sPE by five CRs, or ~15 nm. Measured binding kinetics between the RBCs modified either with selectin construct or with neutrophils displaying PSGL-1 demonstrated that the increased length of the sP increased the binding rate by a factor of 1.9, but the dissociation rates of both proteins were similar. Similarly, the 2D affinity of sP was 2.3-fold higher than that of the sPE form. This rate enhancement derives from the length-dependent increase in the reaction cross-section of the selectin (116).

Consequences of these length-dependent binding differences are apparent in studies of cell or particle capture under flow, where the association kinetics affects capture efficiency. Under static conditions, there is no apparent difference between neutrophil adhesion to surfaces coated with either sPE or sP at similar densities, but under flow, only the longer sP construct supported neutrophil rolling. P-selectin requires at least five CRs to support rolling (117). Similarly, CD2 and its ligands bind at intermembrane distances of 15 nm, a feature that enhances T lymphocyte binding (14). Receptor tethering on flexible polymer chains also enhances liposome adhesion under flow, with consequences for drug targeting to vascular tissues (101, 118).

6. CONCLUDING REMARKS

This review is only a snapshot of the rapidly evolving field of protein nanomechanics. Simulations and sensitive force measurements have identified unique physical properties of adhesion proteins and have proved to be powerful tools for defining the molecular design rules of these complex molecular machines. Although this review focused on adhesion protein mechanochemistry, the exploding interest in the mechanics of biological materials ensures the continued steep trajectory of this field.

SUMMARY POINTS

1. Sensitive force measurement techniques and atomistic simulations identified force-dependent properties of adhesion proteins that are not accessible from crystal structures, solution binding measurements, or standard cell adhesion measurements.

2. Force measurements identify the molecular-level properties that govern cell adhesion at the macroscale.
3. The response of receptor-ligand bonds to time-varying forces depends on the force history. This feature is used both to distinguish between different bound states and to identify different force-dependent dissociation paths.
4. Atomic force microscopy, surface force apparatus, and micropipette manipulation measurements probe different, complementary properties of receptor-ligand bonds. In the cadherin example, the use of all three of these approaches identified different cadherin binding interactions, mapped them to different structural regions of the proteins, and determined their roles in intercellular adhesion.
5. When combined with protein engineering, these complementary theoretical and experimental approaches are powerful tools for defining how protein structures carry out complex mechanical functions.

FUTURE ISSUES

1. Physical adhesion between cell surface proteins and their cognate receptors is only one of the many functions of cell adhesion proteins. Many adhesion proteins are also signaling molecules. A challenge is to determine how the magnitude and duration of adhesion relates to the intracellular signaling that controls cell functions.
2. Adhesion proteins can also act as force sensors that probe their mechanical environments and proportionally modulate cell functions. In such cases, the strength of protein bonds may be less important than the capacity of the proteins to actuate changes in membrane tension or to recruit other components to adhesive contacts in order to strengthen cell adhesion.
3. Adhesion proteins do not operate in isolation. How does cross-talk between different adhesion proteins regulate adhesion-related functions?
4. How does the spatial distribution of adhesion proteins contribute to cell morphology and cell function?

DISCLOSURE STATEMENT

The author is not aware of any affiliations, memberships, funding, or financial holdings that might be perceived as affecting the objectivity of this review.

ACKNOWLEDGMENTS

I thank my colleagues for their generous contributions of illustrations and for useful discussions regarding material presented in this article. I apologize to the many people whose excellent contributions to the field could not be included owing to space limitations. D.L. also acknowledges the National Institutes of Health and the National Science Foundation for support of past and present work.

LITERATURE CITED

1. Maruthamuthu V, Schulten K, Leckband D. 2009. Elasticity and rupture of a multi-domain neural cell adhesion molecule complex. *Biophys. J.* 96:3005–14
2. Craig D, Gao M, Schulten K, Vogel V. 2004. Structural insights into how the MIDAS ion stabilizes integrin binding to an RGD peptide under force. *Structure* 12:2049–58
3. Lou J, Zhu C. 2007. A structure-based sliding-rebinding mechanism for catch bonds. *Biophys. J.* 92:1471–85
4. Gunnerson KN, Pereverzev YV, Prezhdo OV. 2009. Atomistic simulation combined with analytic theory to study the response of the P-selectin/PSGL-1 complex to an external force. *J. Phys. Chem. B* 113:2090–100
5. Bayas MV, Schulten K, Leckband D. 2003. Forced detachment of the CD2-CD58 complex. *Biophys. J.* 84:2223–33
6. Bayas MV, Schulten K, Leckband D. 2004. Forced dissociation of the strand dimer interface between C-cadherin ectodomains. *Mech. Chem. Biosyst.* 1:101–11
7. Sotomayor M, Schulten K. 2008. The allosteric role of the Ca^{2+} switch in adhesion and elasticity of C-cadherin. *Biophys. J.* 94:4621–33
8. Yago T, Lou J, Wu T, Yang J, Miner JJ, et al. 2008. Platelet glycoprotein Ibα forms catch bonds with human WT vWF but not with type 2B von Willebrand disease vWF. *J. Clin. Investig.* 118:3195–207
9. Krammer A, Craig D, Thomas WE, Schulten K, Vogel V. 2002. A structural model for force regulated integrin binding to fibronectin's RGD-synergy site. *Matrix Biol.* 21:139–47
10. del Rio A, Perez-Jimenez R, Liu R, Roca-Cusachs P, Fernandez JM, Sheetz MP. 2009. Stretching single talin rod molecules activates vinculin binding. *Science* 323:638–41
11. Krammer A, Lu H, Isralewitz B, Schulten K, Vogel V. 1999. Forced unfolding of the fibronectin type III module reveals a tensile molecular recognition switch. *Proc. Natl. Acad. Sci. USA* 96:1351–56
12. Sotomayor M, Schulten K. 2007. Single-molecule experiments in vitro and in silico. *Science* 316:1144–48
13. Davis SJ, Ikemizu S, Evans EJ, Fugger L, Bakker TR, van der Merwe PA. 2003. The nature of molecular recognition by T cells. *Nat. Immunol.* 4:217–24
14. van der Merwe PA, Davis SJ. 2003. Molecular interactions mediating T cell antigen recognition. *Annu. Rev. Immunol.* 21:659–84
15. Davis SJ, van der Merwe PA. 1996. The structure and ligand interactions of CD2: implications for T-cell function. *Immunol. Today* 17:177–87
16. Jones EY, Davis SJ, Williams AF, Harlos K, Stuart DI. 1992. Crystal structre at 2.8 Å resolution of a soluble form of the cell adhesion molecule CD2. *Nature* 360:232–39
17. Wang JH, Smolyar A, Tan K, Liu JH, Kim M, et al. 1999. Structure of a heterophilic adhesion complex between the human CD2 and CD58 (LFA-3) counterreceptors. *Cell* 97:791–803
18. Ikemizu S, Sparks LM, van der Merwe PA, Harlos K, Stuart DI, et al. 1999. Crystal structure of the CD2-binding domain of CD58 (lymphocyte function-associated antigen 3) at 1.8-Å resolution. *Proc. Natl. Acad. Sci. USA* 96:4289–94
19. McAlister MSB, Mott HR, van der Merwe PA, Campbell ID, Davis SJ, Driscoll PC. 1996. NMR analysis of interacting soluble forms of the cell–cell recognition molecules CD2 and CD48. *Biochemistry* 35:5982–91
20. Davis SJ, Davies EA, Tucknott MG, Jones EY, van der Merwe A. 1998. The role of charged residues mediating low affinity protein–protein recognition at the cell surface by CD2. *Proc. Natl. Acad. Sci. USA* 95:5490–94
21. Bayas MV, Kearney A, Avramovic A, van der Merwe PA, Leckband DE. 2007. Impact of salt bridges on the equilibrium binding and adhesion of human CD2 and CD58. *J. Biol. Chem.* 282:5589–96
22. Puklin-Faucher E, Gao M, Schulten K, Vogel V. 2006. How the headpiece hinge angle is opened: new insights into the dynamics of integrin activation. *J. Cell Biol.* 175:349–60
23. Bell GI. 1978. Models for the specific adhesion of cells to cells. *Science* 200:618–27
24. Evans E, Ritchie K. 1997. Dynamic strength of molecular adhesion bonds. *Biophys. J.* 72:1541–55
25. Dudko OK, Hummer G, Szabo A. 2008. Theory, analysis, and interpretation of single-molecule force spectroscopy experiments. *Proc. Natl. Acad. Sci. USA* 105:15755–60

26. Dudko OK, Hummer G, Szabo A. 2006. Intrinsic rates and activation free energies from single-molecule pulling experiments. *Phys. Rev. Lett.* 96:108101
27. Hummer G, Szabo A. 2005. Free energy surfaces from single-molecule force spectroscopy. *Acc. Chem. Res.* 38:504–13
28. Dudko OK, Mathe J, Szabo A, Meller A, Hummer G. 2007. Extracting kinetics from single-molecule force spectroscopy: nanopore unzipping of DNA hairpins. *Biophys. J.* 92:4188–95
29. Bayas MV, Leung A, Evans E, Leckband D. 2006. Lifetime measurements reveal kinetic differences between homophilic cadherin bonds. *Biophys. J.* 90:1385–95
30. Perret E, Leung A, Feracci H, Evans E. 2004. *Trans*-bonded pairs of E-cadherin exhibit a remarkable hierarchy of mechanical strengths. *Proc. Natl. Acad. Sci. USA* 101:16472–77
31. Marshall BT, Sarangapani KK, Lou J, McEver RP, Zhu C. 2005. Force history dependence of receptor-ligand dissociation. *Biophys. J.* 88:1458–66
32. Socci ND, Onuchic JN, Wolynes PG. 1999. Stretching lattice models of protein folding. *Proc. Natl. Acad. Sci. USA* 96:2031–35
33. Li F, Leckband D. 2006. Dynamic strength of molecularly bonded surfaces. *J. Chem. Phys.* 125:194702
34. Seifert U. 2000. Rupture of multiple parallel molecular bonds under dynamic loading. *Phys. Rev. Lett.* 84:2750–53
35. Evans E, Ritchie K, Merkel R. 1995. Sensitive force technique to probe molecular adhesion and structural linkages at biological interfaces. *Biophys. J.* 68:2580–87
36. Shi Q, Chien YH, Leckband D. 2008. Biophysical properties of cadherin bonds do not predict cell sorting. *J. Biol. Chem.* 283:28454–63
37. Wieland JA, Gewirth AA, Leckband DE. 2005. Single-molecule measurements of the impact of lipid phase behavior on anchor strengths. *J. Phys. Chem. B* 109:5985–93
38. Weisel JW, Shuman H, Litvinov RI. 2003. Protein–protein unbinding induced by force: single-molecule studies. *Curr. Opin. Struct. Biol.* 13:227–35
39. Evans E, Kinoshita K. 2007. Using force to probe single-molecule receptor-cytoskeletal anchoring beneath the surface of a living cell. *Methods Cell Biol.* 83:373–96
40. Evans E, Heinrich V, Leung A, Kinoshita K. 2005. Nano- to microscale dynamics of P-selectin detachment from leukocyte interfaces. I. Membrane separation from the cytoskeleton. *Biophys. J.* 88:2288–98
41. Muller DJ. 2008. AFM: a nanotool in membrane biology. *Biochemistry* 47:7986–98
42. Puchner EM, Gaub HE. 2009. Force and function: probing proteins with AFM-based force spectroscopy. *Curr. Opin. Struct. Biol.* 19:605–14
43. Borgia A, Williams PM, Clarke J. 2008. Single-molecule studies of protein folding. *Annu. Rev. Biochem.* 77:101–25
44. Marshall BT, Long M, Piper JW, Yago T, McEver RP, Zhu C. 2003. Direct observation of catch bonds involving cell-adhesion molecules. *Nature* 423:190–93
45. Alon R, Hammer DA, Springer TA. 1995. Lifetime of the P-selectin-carbohydrate bond and its response to tensile force in hydrodynamic flow. *Nature* 374:539–42
46. Evans E, Leung A, Hammer D, Simon S. 2001. Chemically distinct transition states govern rapid dissociation of single L-selectin bonds under force. *Proc. Natl. Acad. Sci. USA* 98:3784–89
47. Evans E, Leung A, Heinrich V, Zhu C. 2004. Mechanical switching and coupling between two dissociation pathways in a P-selectin adhesion bond. *Proc. Natl. Acad. Sci. USA* 101:11281–86
48. Zhu C, McEver RP. 2005. Catch bonds: physical models and biological functions. *Mol. Cell Biomech.* 2:91–104
49. Yago T, Wu J, Wey CD, Klopocki AG, Zhu C, McEver RP. 2004. Catch bonds govern adhesion through L-selectin at threshold shear. *J. Cell Biol.* 166:913–23
50. Sarangapani KK, Yago T, Klopocki AG, Lawrence MB, Fieger CB, et al. 2004. Low force decelerates L-selectin dissociation from P-selectin glycoprotein ligand-1 and endoglycan. *J. Biol. Chem.* 279:2291–98
51. Yago T, Zarnitsyna VI, Klopocki AG, McEver RP, Zhu C. 2007. Transport governs flow-enhanced cell tethering through L-selectin at threshold shear. *Biophys. J.* 92:330–42
52. Dembo M, Torney DC, Saxman K, Hammer D. 1988. The reaction-limited kinetics of membrane-to-surface adhesion and detachment. *Proc. R. Soc. London Ser. B* 234:55–83

53. Finger EB, Puri KD, Alon R, Lawrence MB, von Andrian UH, Springer TA. 1996. Adhesion through L-selectin requires a threshold hydrodynamic shear. *Nature* 379:266–69
54. Pierres A, Benoliel AM, Bongrand P. 1996. Measuring bonds between surface-associated molecules. *J. Immunol. Methods* 196:105–20
55. Thomas WE, Trintchina E, Forero M, Vogel V, Sokurenko EV. 2002. Bacterial adhesion to target cells enhanced by shear force. *Cell* 109:913–23
56. Yakovenko O, Sharma S, Forero M, Tchesnokova V, Aprikian P, et al. 2008. FimH forms catch bonds that are enhanced by mechanical force due to allosteric regulation. *J. Biol. Chem.* 283:11596–605
57. Kong F, Garcia AJ, Mold AP, Humphries MJ, Zhu C. 2009. Demonstration of catch bonds between an integrin and its ligand. *J. Cell Biol.* 185:1275–84
58. Zhu C, Lou J, McEver RP. 2005. Catch bonds: physical models, structural bases, biological function and rheological relevance. *Biorheology* 42:443–62
59. Zhu C, Yago T, Lou J, Zarnitsyna VI, McEver RP. 2008. Mechanisms for flow-enhanced cell adhesion. *Ann. Biomed. Eng.* 36:604–21
60. Thomas W. 2008. Catch bonds in adhesion. *Annu. Rev. Biomed. Eng.* 10:39–57
61. Thomas WE, Vogel V, Sokurenko E. 2008. Biophysics of catch bonds. *Annu. Rev. Biophys.* 37:399–416
62. Prezhdo OV, Pereverzev YV. 2009. Theoretical aspects of the biological catch bond. *Acc. Chem. Res.* 42:693–703
63. Pereverzev YV, Prezhdo OV, Forero M, Sokurenko EV, Thomas WE. 2005. The two-pathway model for the catch-slip transition in biological adhesion. *Biophys. J.* 89:1446–54
64. Barsegov V, Thirumalai D. 2005. Dynamics of unbinding of cell adhesion molecules: transition from catch to slip bonds. *Proc. Natl. Acad. Sci. USA* 102:1835–39
65. Aprikian P, Tchesnokova V, Kidd B, Yakovenko O, Yarov-Yarovoy V, et al. 2007. Interdomain interaction in the FimH adhesin of *Escherichia coli* regulates the affinity to mannose. *J. Biol. Chem.* 282:23437–46
66. Thomas WE. 2009. Mechanochemistry of receptor-ligand bonds. *Curr. Opin. Struct. Biol.* 19:50–55
67. Phan UT, Waldron TT, Springer TA. 2006. Remodeling of the lectin-EGF-like domain interface in P- and L-selectin increases adhesiveness and shear resistance under hydrodynamic force. *Nat. Immunol.* 7:883–89
68. Waldron TT, Springer TA. 2009. Transmission of allostery through the lectin domain in selectin-mediated cell adhesion. *Proc. Natl. Acad. Sci. USA* 106:85–90
69. Lou J, Yago T, Klopocki AG, Mehta P, Chen W, et al. 2006. Flow-enhanced adhesion regulated by a selectin interdomain hinge. *J. Cell Biol.* 174:1107–17
70. Chothia C, Jones EY. 1997. The molecular structure of cell adhesion molecules. *Annu. Rev. Biochem.* 66:823–62
71. Walsh FS, Doherty P. 1997. Neural cell adhesion molecules of the immunoglobulin superfamily: role in axon growth and guidance. *Annu. Rev. Cell Dev. Biol.* 13:425–56
72. Yap AS, Brieher WM, Pruschy M, Gumbiner BM. 1997. Lateral clustering of the adhesive ectodomain: a fundamental determinant of cadherin function. *Curr. Biol.* 7:308–15
73. Brieher WM, Yap AS, Gumbiner BM. 1996. Lateral dimerization is required for the homophilic binding activity of C-cadherin. *J. Cell Biol.* 135:487–96
74. Tsukasaki Y, Kitamura K, Shimizu K, Iwane AH, Takai Y, Yanagida T. 2007. Role of multiple bonds between the single cell adhesion molecules, nectin and cadherin, revealed by high sensitive force measurements. *J. Mol. Biol.* 367:996–1006
75. Sivasankar S, Zhang Y, Nelson WJ, Chu S. 2009. Characterizing the initial encounter complex in cadherin adhesion. *Structure* 17:1075–81
76. Soroka V, Kolkova K, Kastrup JS, Diederichs K, Breed J, et al. 2003. Structure and interactions of NCAM Ig1–2–3 suggest a novel zipper mechanism for homophilic adhesion. *Structure* 11:1291–301
77. Kasper C, Rasmussen H, Kastrup JS, Ikemizu S, Jones EY, et al. 2000. Structural basis of cell–cell adhesion by NCAM. *Nat. Struct. Biol.* 7:389–93
78. Wieland JA, Gewirth AA, Leckband DE. 2005. Single molecule adhesion measurements reveal two homophilic neural cell adhesion molecule bonds with mechanically distinct properties. *J. Biol. Chem.* 280:41037–46

79. Johnson CP, Fujimoto I, Perrin-Tricaud C, Rutishauser U, Leckband D. 2004. Mechanism of homophilic adhesion by the neural cell adhesion molecule: use of multiple domains and flexibility. *Proc. Natl. Acad. Sci. USA* 101:6963–68
80. Hynes RO. 2002. Integrins: bidirectional, allosteric signaling machines. *Cell* 110:673–87
81. Helenius J, Heisenberg CP, Gaub HE, Muller DJ. 2008. Single-cell force spectroscopy. *J. Cell Sci.* 121:1785–91
82. Benoit M, Gabriel D, Gerisch G, Gaub HE. 2000. Discrete interactions in cell adhesion measured by single-molecule force spectroscopy. *Nat. Cell Biol.* 2:313–17
83. Leckband D, Israelachvili J. 2001. Intermolecular forces in biology. *Q. Rev. Biophys.* 34:105–267
84. Israelachvili J. 1973. Thin film studies using multiple-beam interferometry. *J. Colloid Interface Sci.* 44:259–72
85. Israelachvili J, McGuiggan P. 1990. Adhesion and short-range forces between surfaces: new apparatus for surface force measurements. *J. Mater. Res.* 5:2223–31
86. Hunter R. 1989. *Foundations of Colloid Science*. Oxford, UK: Oxford Univ. Press
87. Israelachvili J. 1992. *Intermolecular and Surface Forces*. New York: Academic
88. Leckband DE, Schmitt FJ, Israelachvili JN, Knoll W. 1994. Direct force measurements of specific and nonspecific protein interactions. *Biochemistry* 33:4611–24
89. Leckband D, Muller W, Schmitt FJ, Ringsdorf H. 1995. Molecular mechanisms determining the strength of receptor-mediated intermembrane adhesion. *Biophys. J.* 69:1162–69
90. Yeung C, Purves T, Kloss AA, Kuhl TL, Sligar S, Leckband D. 1999. Cytochrome *c* recognition of immobilized, orientational variants of cytochrome *b*5: direct force and equilibrium binding measurements. *Langmuir* 15:6829–36
91. Leckband DE, Kuhl T, Wang HK, Herron J, Muller W, Ringsdorf H. 1995. 4-4-20 antifluorescyl IgG Fab′ recognition of membrane bound hapten: direct evidence for the role of protein and interfacial structure. *Biochemistry* 34:11467–78
92. Zhu B, Davies EA, van der Merwe PA, Calvert T, Leckband DE. 2002. Direct measurements of heterotypic adhesion between the cell surface proteins CD2 and CD48. *Biochemistry* 41:12163–70
93. Geijtenbeek TB, Engering A, Van Kooyk Y. 2002. DC-SIGN, a C-type lectin on dendritic cells that unveils many aspects of dendritic cell biology. *J. Leukoc. Biol.* 71:921–31
94. Geijtenbeek T, Kwon D, Torensma R, van Vliet S, van Duijnhoven G, et al. 2000. DC-SIGN, a dendritic cell-specific HIV-1-binding protein that enhances *trans*-infection of T cells. *Cell* 100:587–97
95. van Kooyk Y, Geijtenbeek T. 2003. DC-SIGN: escape mechanism for pathogens. *Nat. Rev. Immunol.* 3:697–709
96. Feinberg H, Guo Y, Mitchell D, Drickamer K, Weis W. 2005. Extended neck regions stabilize tetramers of the receptors DC-SIGN and DC-SIGNR. *J. Biol. Chem.* 280:1327–35
97. Menon S, Rosenberg K, Graham SA, Ward EM, Taylor ME, et al. 2009. Binding-site geometry and flexibility in DC-SIGN demonstrated with surface force measurements. *Proc. Natl. Acad. Sci. USA* 106:11524–29
98. Wong JY, Kuhl TL. 2008. Dynamics of membrane adhesion: the role of polyethylene glycol spacers, ligand-receptor bond strength, and rupture pathway. *Langmuir* 24:1225–31
99. Wong JY, Kuhl TL, Israelachvili JN, Mullah N, Zalipsky S. 1997. Direct measurement of a tethered ligand-receptor interaction potential. *Science* 275:820–22.
100. Jeppesen C, Wong JY, Kuhl TL, Israelachvili JN, Mullah N, et al. 2001. Impact of polymer tether length on multiple ligand-receptor bond formation. *Science* 293:465–68
101. Ham AS, Klibanov AL, Lawrence MB. 2009. Action at a distance: lengthening adhesion bonds with poly(ethylene glycol) spacers enhances mechanically stressed affinity for improved vascular targeting of microparticles. *Langmuir* 25:10038–44
102. Leckband D. 2008. From single molecules to living cells: nanomechanical measurements of cell adhesion. *Cell Mol. Bioeng.* 1:312–26
103. Leckband D. 2008. Beyond structure: mechanism and dynamics of intercellular adhesion. *Biochem. Soc. Trans.* 36:213–20
104. Zhu B, Chappuis-Flament S, Wong E, Jensen IE, Gumbiner BM, Leckband D. 2003. Functional analysis of the structural basis of homophilic cadherin adhesion. *Biophys. J.* 84:4033–42

105. Chien YH, Jiang N, Li F, Zhang F, Zhu C, Leckband D. 2008. Two stage cadherin kinetics require multiple extracellular domains but not the cytoplasmic region. *J. Biol. Chem.* 283:1848–56
106. Chesla SE, Selvaraj P, Zhu C. 1998. Measuring two-dimensional receptor-ligand binding kinetics by micropipette. *Biophys. J.* 75:1553–72
107. Evans E, Berk D, Leung A. 1991. Detachment of agglutinin-bonded red blood cells. I. Forces to rupture molecular-point attachments. *Biophys. J.* 59:838–48
108. Zhang F, Marcus WD, Goyal NH, Selvaraj P, Springer TA, Zhu C. 2005. Two-dimensional kinetics regulation of αLβ2-ICAM-1 interaction by conformational changes of the αL-inserted domain. *J. Biol. Chem.* 280:42207–18
109. Zhu C, Long M, Chesla SE, Bongrand P. 2002. Measuring receptor/ligand interaction at the single-bond level: experimental and interpretative issues. *Ann. Biomed. Eng.* 30:305–14
110. Chesla SE, Li P, Nagarajan S, Selvaraj P, Zhu C. 2000. The membrane anchor influences ligand binding two-dimensional kinetic rates and three-dimensional affinity of FcγRIII (CD16). *J. Biol. Chem.* 275:10235–46
111. Long M, Zhao H, Huang KS, Zhu C. 2001. Kinetic measurements of cell surface E-selectin/carbohydrate ligand interactions. *Ann. Biomed. Eng.* 29:935–46
112. Williams TE, Nagarajan S, Selvaraj P, Zhu C. 2000. Concurrent and independent binding of Fcγ receptors IIa and IIIb to surface-bound IgG. *Biophys. J.* 79:1867–75
113. Williams TE, Nagarajan S, Selvaraj P, Zhu C. 2001. Quantifying the impact of membrane microtopology on effective two-dimensional affinity. *J. Biol. Chem.* 276:13283–88
114. Mohandas N, Evans E. 1984. Adherence of sickle erythrocytes to vascular endothelial cells: requirement for both cell membrane changes and plasma factors. *Blood* 64:282–87
115. Boggon TJ, Murray J, Chappuis-Flament S, Wong E, Gumbiner BM, Shapiro L. 2002. C-cadherin ectodomain structure and implications for cell adhesion mechanisms. *Science* 296:1308–13
116. Huang J, Chen J, Chesla SE, Yago T, Mehta P, et al. 2004. Quantifying the effects of molecular orientation and length on two-dimensional receptor-ligand binding kinetics. *J. Biol. Chem.* 279:44915–23
117. Patel KD, Nollert MU, McEver RP. 1995. P-selectin must extend a sufficient length from the plasma membrane to mediate rolling of neutrophils. *J. Cell Biol.* 131:1893–902
118. Duncanson WJ, Figa MA, Hallock K, Zalipsky S, Hamilton JA, Wong JY. 2007. Targeted binding of PLA microparticles with lipid-PEG-tethered ligands. *Biomaterials* 28:4991–99

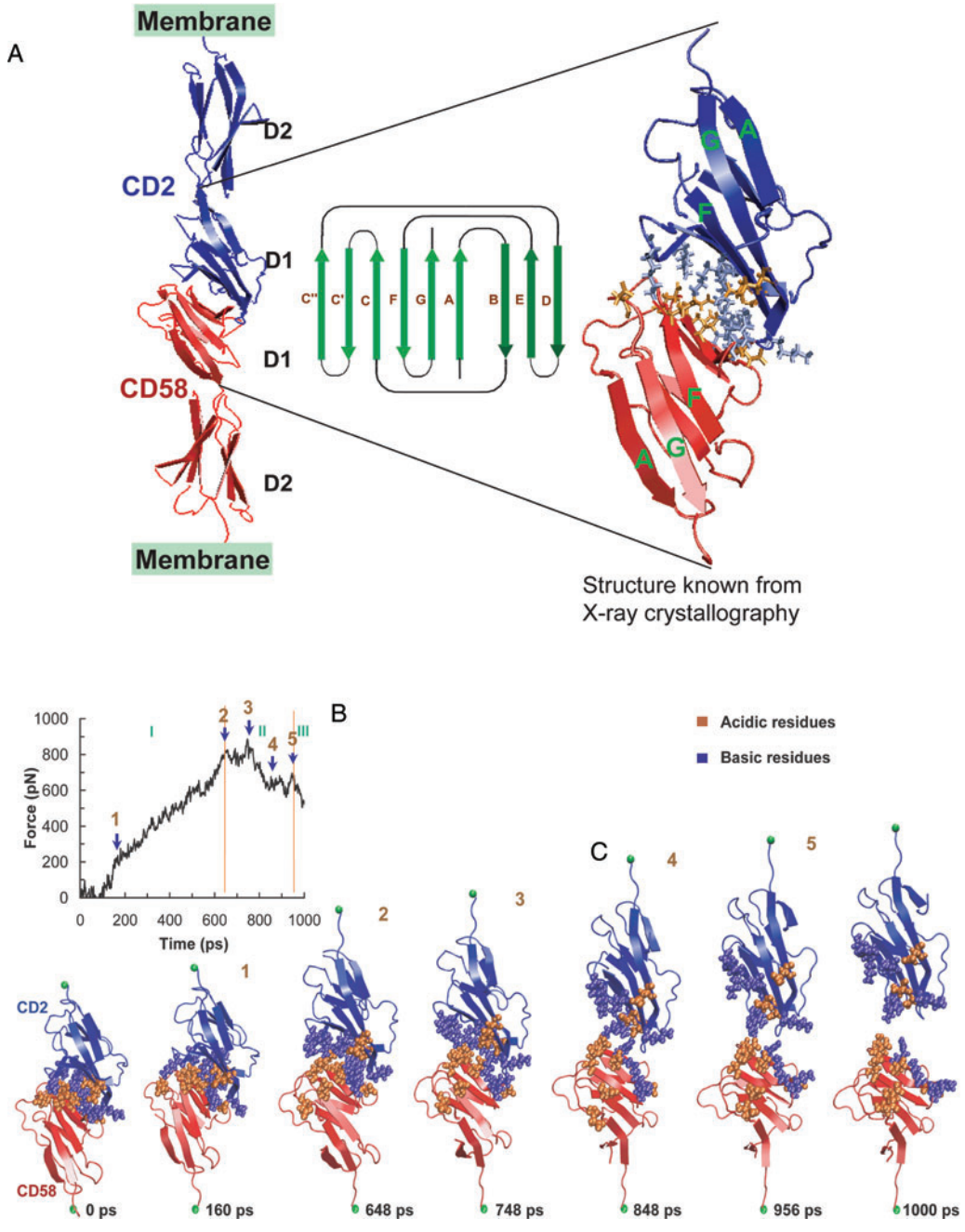

Figure 1

(*A*) Model of the CD2–CD58 complex based on the crystal structure of the complex of the two outer D1 domains of CD2 and CD58 (*right*). (*B*) Simulated force on the protein complex as a function of the simulation time. The pulling rate is ~0.2 pN ps^{-1}. The discontinuities in the trajectory indicate intermolecular bond failure. (*C*) Snapshots of the protein complex at points in the simulation correspond to the indicated discontinuities in the force-time plot in (*B*).

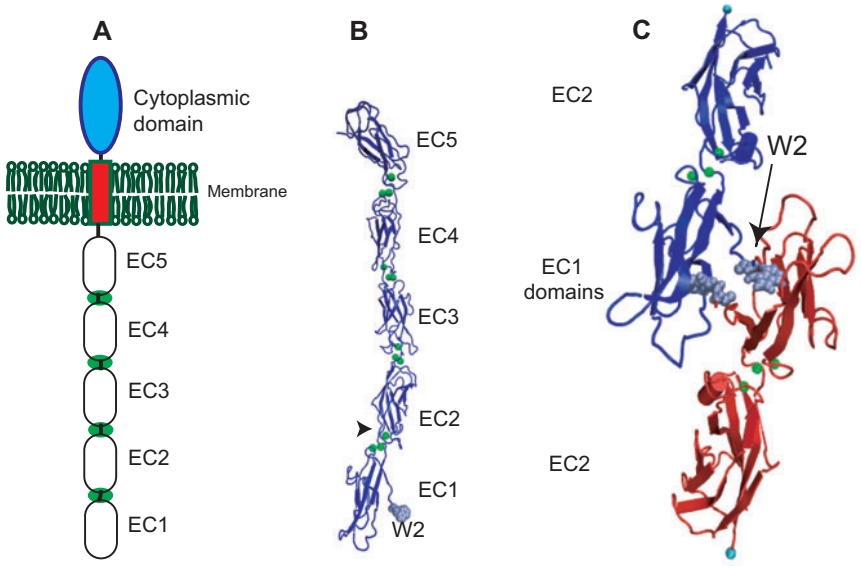

Figure 4

Classical cadherin structure and binding model. (*A*) The classical cadherins are transmembrane proteins with a cytoplasmic domain, a transmembrane region, and an ectodomain. The ectodomain folds into five structurally homologous ECs numbered 1–5 from the N-terminus. (*B*) Crystal structure of the ectodomain of *Xenopus* C-cadherin. (*C*) Binding between N-terminal domains of the C-cadherin ectodomain in which the tryptophan at position 2 (W2) from opposing cadherins docks into the hydrophobic pocket of the other protein.

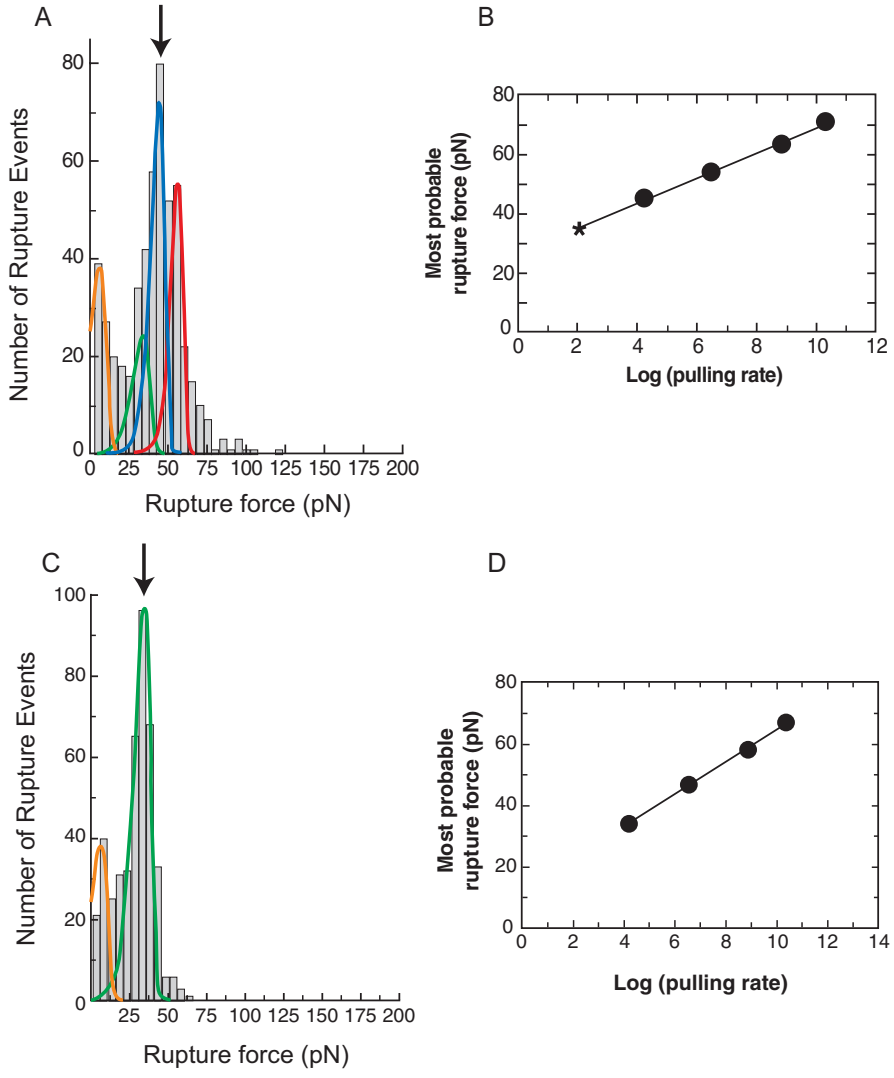

Figure 5

Single bond rupture measurements with C-cadherin ectodomain fragments (CEC) 12 Fc and CEC1–5 Fc. (*A*) Force histogram measured between CEC1–5 Fc fragments at $r_F = 69$ pN s^{-1}. The orange, green, blue, and red curves are the distributions calculated by fitting the histograms to a superposition of four probability distributions that correspond to four independent bonds. (*B*) Most probable rupture force F_{mp} for the peak indicated by the arrow in (*A*) versus log (r_F). (*C*) Force histogram measured with CEC12 Fc fragments at $r_F = 68$ pN s^{-1}. The orange and green curves are the distributions calculated with the experimentally determined parameters for each bond contributing to the histogram. These correspond with the orange and green peaks measured with CEC1–5 Fc in (*A*). (*D*) Most probable rupture force F_{mp} for the peak indicated by the arrow in (*C*) versus log (r_F).

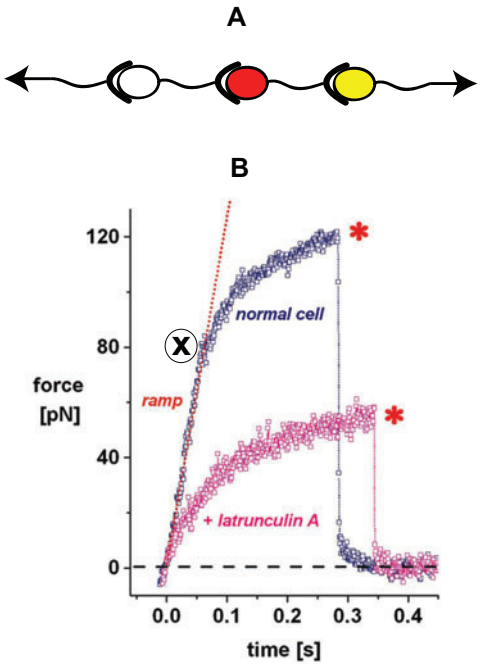

Figure 6

Probing P-selectin cytoskeletal linkages with the biomembrane force probe (BFP). (*A*) Schematic of multiple bonds in series. (*B*) P-selectin on a leukocyte was pulled away from P-selectin-glycoprotein-ligand-1 (PSGL-1) immobilized on a bead. In the absence of latrunculin A (organized actin cytoskeleton), bonds subjected to a steady ramp force initially exhibited a linear force-time curve. The data deviate from the linear ramp, and the pulling rate slows at ⊗, upon rupture of the P-selectin-cytoskeleton bond. At ∗, the P-selectin/PSGL-1 bond fails. Latrunculin A disrupts actin and prevents P-selectin binding to the cytoskeleton. With cells treated with latrunculin A, the force-time trajectory exhibits only the viscous drag owing to the lipid nanotube extraction and the final P-selectin/PSGL-1 bond rupture.

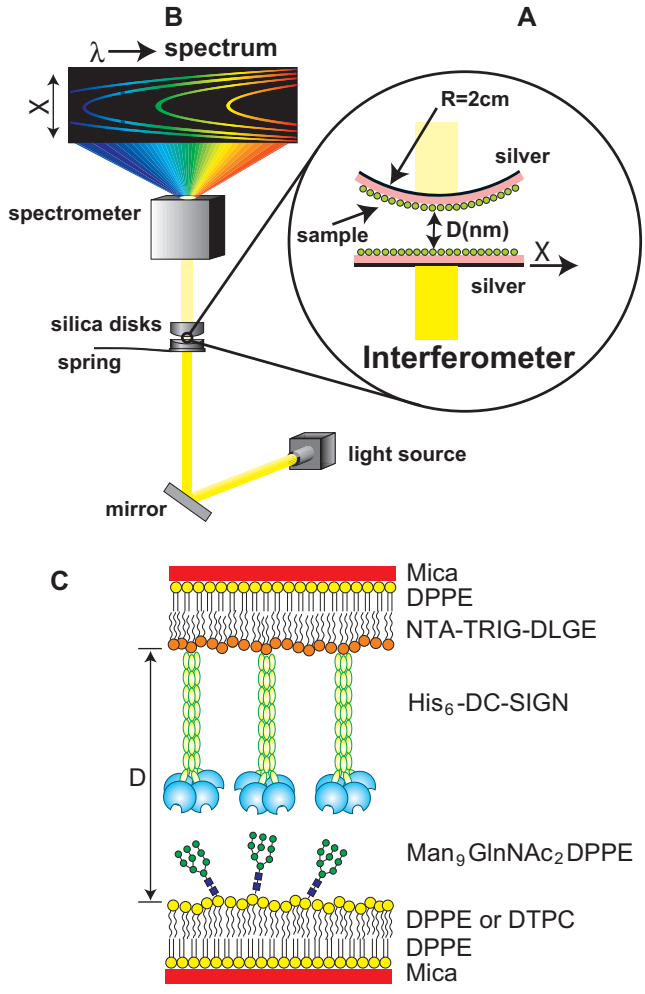

Figure 7

Principles of surface force apparatus (SFA) measurements (83). (*A*) Schematic of the samples in the interferometer of the SFA. The samples are supported on two hemicylindrical lenses oriented at right angles to each other. The equivalent geometry is a sphere interacting with a flat plate, as indicated here. The samples, e.g., proteins, are on the surfaces of the two lenses. *X* indicates the radial distance from the center of contact, where the surface separation distance is *D*. (*B*) Interference fringes transmitted by the interferometer. The curvature of the fringes images the curvature of the contact region. *X* corresponds to the radial distance from the center of contact, as in (*A*). (*C*) Example of a typical sample configuration used in the surface force apparatus experiment. In this example, the protein dendritic cell-specific integrin grabbing nonintegrin (DC-SIGN) is immobilized via a hexahistidine tail (His_6) at the N-terminus (DC-SIGN-His_6). The hexahistidine tail binds to 6-[9-[2,3-bis(dodecyloxy)propyl]-3,6,9-trioxanonyl-1-oxycarboxylamino]-2-[di(carboxymethyl)-amino]-hexanoic acid (NTA-TRIG-DLGE) in the outer leaflet of the supported bilayer. The opposing membrane contains a synthetic lipid with the glycan (ligand) head group. *D* is the absolute separation between the bilayer surfaces. $Man_9GlnNAc_2$ is a carbohydrate (glycan) consisting of a core of two *N*-acetyl-glucosamine ($GlnNAc_2$) sugars coupled to a branched carbohydrate consisting of nine mannose sugars (Man_9). Abbreviations: DPPE, 1,2-dipalmitoyl-*sn*-glycero-3-phosphoethanolamine; DTPC, 1,2-ditridecanoyl-sn-glycero-3-phosphocholine.

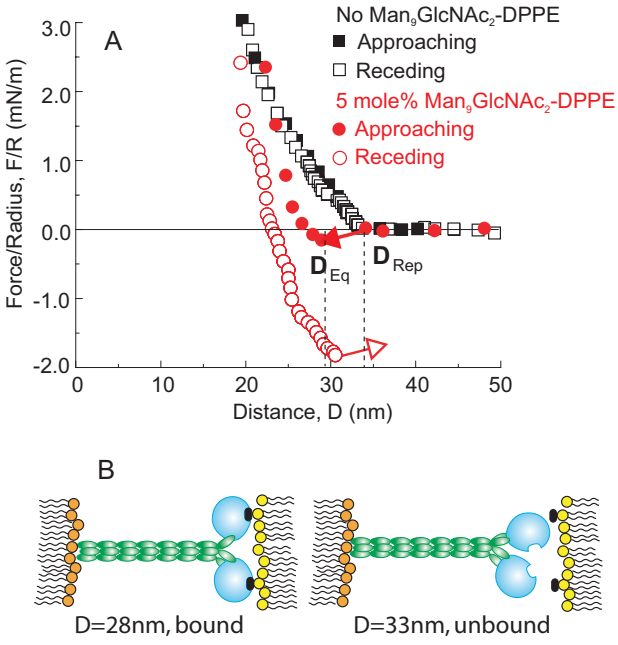

Figure 8

(*A*) Normalized force versus the distance between membranes displaying DC-SIGN ectodomains and supported lipid bilayers with and without glycan ligand. The sample configuration is shown in **Figure 7*C***. The black squares show the approaching (*open squares*) and receding (*filled squares*) force measurements in the absence of glycan ligand. The red circles show the approaching (*filled circles*) and receding (*open circles*) force curves in the presence of glycan. The arrows show where the jump instabilities occur. At these points, the surfaces jump into or out of adhesive contact. Here D_{Eq} is the equilibrium separation at which the surfaces come to rest after jumping to contact. D_{Rep} is the position of the onset of steric repulsion between the two surfaces. (*B*) Schematic of proposed DC-SIGN configuration and conformational change upon ligand binding. The blue circles represent the carbohydrate recognition domains, and the chains of green ellipsoids represent the neck region.

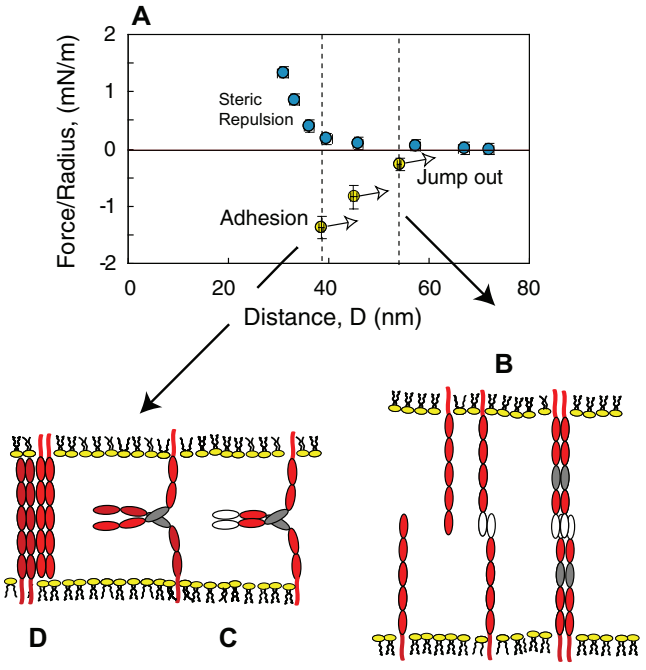

Figure 10

(*A*) Force normalized by the radius (*F/R*) versus the distance *D* between lipid bilayers supporting oriented cadherin monolayers. The blue circles indicate the normalized force during approach, and the yellow circles show the three distances at which the protein monolayers adhere. The open arrows indicate the positions from which the protein layers jump out of adhesive contact. The illustration shows possible protein configurations corresponding to (*B*), the outer adhesive minimum at 55 nm, and (*C*), possible *cis* EC3 alignments consistent with the adhesion at 39 nm. (*D*) Interdigitated cadherin configuration consistent with *trans* (antiparallel) EC3 alignment and adhesion at 39 nm. In (*B*, *C*), white ellipses indicate *trans* bonds between opposing domains, whereas gray ellipses indicate possible *cis* (parallel) domain interactions.

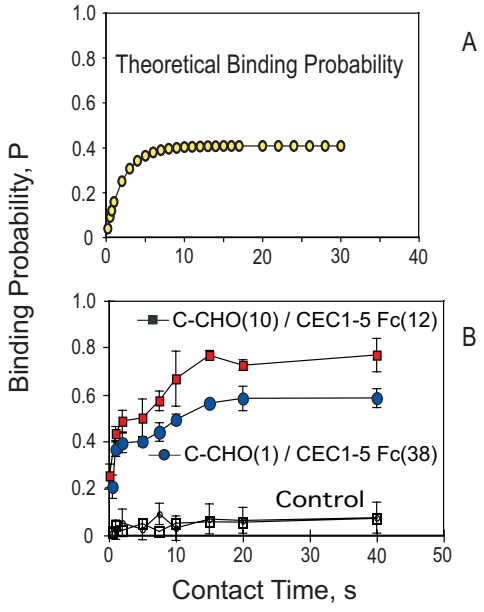

Figure 11

Micropipette measurements of cadherin-mediated cell binding probability versus intercellular contact time. (*A*) Profile of the binding probability *P* versus intercellular contact time predicted for the simple strand exchange binding mechanism (see **Figure 4*C***). (*B*) Experimentally measured binding probability time courses obtained with Chinese hamster ovary (CHO) cells expressing C-cadherin and RBCs modified with the cadherin ectodomain EC1–5Fc (see **Figure 3*E*).** The filled circles and filled squares were measured at different cadherin surface densities on both the CHO and RBC surfaces. The numbers in parentheses are cadherin densities in number of proteins per square micrometer. The open symbols show controls done with ethylene di-amine tetra-acetic acid (EDTA) or blocking antibody, both of which inhibit cadherin binding activity.

Annual Review of Chemical and Biomolecular Engineering

Volume 1, 2010

Contents

Errata

An online log of corrections to *Annual Review of Chemical and Biomolecular Engineering* articles may be found at http://chembioeng.annualreviews.org/errata.shtml